Filomat 38:33 (2024), 11823–11853
https://doi.org/10.2298/FIL2433823M

Published by Faculty of Sciences and Mathematics,
University of Niš, Serbia
Available at: http://www.pmf.ni.ac.rs/filomat

Dynamical analysis of a prey-predator model with specific mortality of predator under the influence of fear felt by prey

Nirmalya Mondal[a], Souvick Karmakar[a], Debgopal Sahoo[a], Guruprasad Samanta[a,*]

[a]*Department of Mathematics, Indian Institute of Engineering Science and Technology, Shibpur, Howrah - 711103, India*

Abstract. Predator-prey interactions are a core component of theoretical ecology, crucial in establishing community structure and preserving ecological diversity. The effect of fear on prey by predator species and the maximal mortality rate of predator species is currently becoming an essential topic in ecology. The present work focuses on a prey-predator model that incorporates a specific mortality function for the predator species and a simplified Holling type IV functional response. Furthermore, the model incorporates an intraspecific competition among individuals of the prey species, the natural mortality rate of prey species, and the effect of fear on the prey population produced by predators in order to get more accurate and realistic dynamics. An analysis is conducted to determine the feasibility and stability conditions of equilibrium points in terms of the model parameters. The condition for the existence of at least one interior equilibrium point has been derived in terms of the model parameters. Several types of local bifurcations have been observed in the system such as transcritical bifurcation, saddle node bifurcation, Bogdanov-Takens bifurcation, Hopf bifurcation, Generalized Hopf bifurcation, Cusp bifurcation, 'Saddle node bifurcation of limit cycle' and a global bifurcation namely Homoclinic Bifurcation is also observed. Furthermore, the effect of hysteresis on our proposed model have been discussed. Numerical simulations have been performed using MATLAB and MATCONT to illustrate our analytical findings.

1. Introduction

Prey-predator interactions are essential ecological connections that have a significant impact on the structure of ecosystems. Due to the complexity of ecosystems, mathematical and experimental ecologists [1, 2] have consistently shown interest to the dynamics of ecosystem. The importance of studying these dynamics gives the insights of these complex ecological processes [3]. Mathematical models are playing an increasingly pivotal role in theoretical ecology, offering valuable contributions not only to the quantitative understanding of ecosystems but also to the advancement of mathematical modelling methodologies. The first prey-predator model was introduced in 1920, followed by the Lotka-Volterra model in 1925. Later, Holling introduced the concept of the functional response, which has since been extensively studied to

2020 *Mathematics Subject Classification*. Primary 92B05; Secondary 92D25, 92D40.
Keywords. Specific mortality function; Fear effect; Generalized Hopf bifurcation; Bogdanov-Takens bifurcation; Homoclinic Bifurcation; Hysteresis.
Received: 04 October 2024; Accepted: 05 October 2024
Communicated by Maria Alessandra Ragusa
Research supported by Indian Institute of Engineering Science and Technology, Shibpur
* Corresponding author: Guruprasad Samanta
Email addresses: nirmalyamondal97@gmail.com (Nirmalya Mondal), skarmakaruttarpara@gmail.com (Souvick Karmakar), debgopalsahoo94@gmail.com (Debgopal Sahoo), g_p_samanta@yahoo.co.uk, gpsamanta@math.iiests.ac.in (Guruprasad Samanta)

understand its impact on prey-predator dynamics. In those models, the functional response is typically assumed to be either prey-dependent or ratio-dependent. Some of these functional responses that are often used are Holling type-I, II, III, IV, Beddington–DeAngelis, Crowley–Martin, and Hassell–Varley [4, 5, 6, 7, 8] etc. A classical prey-predator model incorporating predator functional response on prey population can be written as,

$$\frac{dx}{dt} = \mathcal{H}(x) - \mathcal{F}(x, y)y$$
$$\frac{dy}{dt} = m\mathcal{F}(x, y)y - G(y)y$$

Here x and y represents prey and predator population, $\mathcal{H}(x)$ denotes the intrinsic growth function, $\mathcal{F}(x, y)$ is functional response and $G(y)$ represents the mortality function of predator. In most of the articles the mortality function is considered as $G(y) = \mu$, a constant. However, Cavani and Farkas [9] firstly introduced the specific mortality function as $G(y) = \frac{p+qy}{1+y}$, where p is the mortality of predator at initial density and q is the limiting mortality. This specific mortality function depends on the predator population which is neither constant nor an unbounded function, that is ecologically convenient. Now if $p = q = \mu$, this specific mortality function becomes $G(y) = \mu$, a constant. Juan Ye et al. [10] examined the dynamics of a prey-predator model by incorporating a specific mortality function for the predator species along with a strong Allee effect on the prey population.

In mathematical ecology, "Fear function" refers to the impact of fear on prey species due to the presence of predators. Predators influence prey not only through direct predation but also by inducing fear through behavioral changes in prey, such as reduced foraging, increased vigilance, or habitat shifts. These effects can alter prey population growth, potentially leading to decreased prey numbers even in the absence of direct predation. Wang et al. [11] investigated a model that incorporates prey and predator dynamics, with the impact of fear on prey reproduction, which demonstrates that a significant amount of fear contributes to the stability of the system by eliminating periodic oscillations. Several theoretical and mathematical ecologists [11] conclude that the change in behaviors of prey biomass is greatly influenced by the presence of predators. In some cases, these behavioral changes of prey species are so severe that it becomes more sensitive to form a community structure than direct predation. A 2011 field experiment on song sparrows (Melospiza melodia) by Zanette et al. [12] revealed that fear alone can significantly affect prey populations. By removing direct predation and playing predator sounds to mimic predation risk, the study found a 40% reduction in offspring production. This decline was attributed to anti-predator behaviors, like temporarily abandoning habitats, which disrupted vital activities such as mating. The research suggests that fear can decrease prey fertility and survival, potentially causing larger population declines than direct predation.

In this current study, we have introduced a prey-predator model with a fear function and specific mortality function of predator species. Furthermore, Holling type-IV functional response, natural death rate of prey, and decay rate due to intraspecific competition between prey species have been introduced in the proposed system. In section 2, we have formulated the prey-predator model along with parameters. The positivity and boundedness of the system have been discussed in section 3. Subsequently, the existence and number of equilibrium points have been determined in section 4. Section 5 displays the stability analysis of these equilibrium points. Additionally, we have theoretically examined possible bifurcations in section 6. After that, numerical simulations have been performed in section 7 to learn more about one and two parametric bifurcations. The concept of hysteresis has been discussed in this section. Finally, section 8 provides the conclusion of this work.

2. Model Formulation

In the above classical model incorporating predator functional response on prey population, the logistic growth for prey may be described by three distinct components: the birth rate, denoted as r, the death rate, represented by β, and a reduction due to the competition within the same species, denoted as α. Incorporating these, we get, $\mathcal{H}(x) = (r - \beta)x - \alpha x^2$. Here we consider the Holling type IV [13, 14] functional

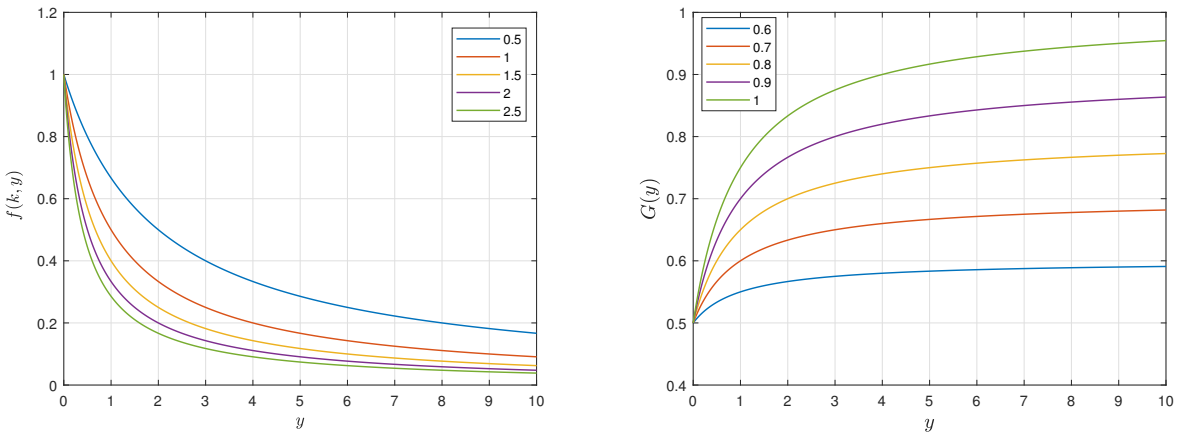

(a) Fear function $f(k, y)$ (b) Specific mortality function $G(y)$

Figure 1: Figure of fear function $f(k, y)$ for $\{k = 0.5, 1, 1.5, 2, 2.5\}$ and specific mortality function $G(y)$ for $\{p = 0.5, q = 0.6, 0.7, 0.8, 0.9, 1\}$.

response $\mathcal{F}(x, y) = \frac{gx}{1+hx^2}$, represents the number of prey consumed by a predator per unit of time. The parameter $m\,(0 < m < 1)$ is the conversion factor, whereas μ denotes the death rate of the predator.

Multiple studies suggest that the presence of a predator, which induces fear in prey species, can significantly reduce their reproductive rate. In some cases, this fear factor has a higher impact on prey depletion than direct predation itself. In this context, the parameter k represents the intensity of fear, influencing the prey's anti-predator behaviors. Given the biological interpretations of k, y, and $f(k, y)$, it is justifiable to conclude that:

$$f(0, y) = 1, \quad f(k, 0) = 1, \quad \frac{\partial f}{\partial k} < 0, \quad \frac{\partial f}{\partial y} < 0,$$

$$\lim_{k\to\infty} f(k, y) = 0, \quad \lim_{y\to\infty} f(k, y) = 0$$

Biologically these implies, in the absence of fear or predators, the reproduction rate of prey species remains unaffected by the fear of a predator. But increasing level of fear or expanding predator population have a detrimental impact on prey reproduction. Moreover, this detrimental effect could increase to a level where the prey population is declining substantially. In specifically, we analyze the fear function $f(k, y) = \dfrac{1}{1 + ky}$. Numerically we have shown the fear function $f(k, y)$ for different values of k in Figure 1a.

Here we consider the Holling type IV functional response, so $\mathcal{F}(x) = \dfrac{gx}{1 + hx^2}$, where g represents predation rate or attacking rate and h determines the decline in consumption rate at high prey densities. Also the specific mortality rate of predators in the absence of prey depends on the number of predators. Now consider the specific mortality function,

$$G(y) = \frac{p + qy}{1 + y}$$

which satisfies the following conditions:

$$G(0) = p, \quad \frac{\partial G}{\partial y} > 0, \quad \lim_{y\to\infty} G(y) = q, \quad G'' < 0$$

where, p and q are described as above and $G(y)$ is convex and increasing function as depicted in Figure 1b for different values of p, q. By the functional properties of $G(y)$ clearly $q > p$, which is also biologically

reasonable. By incorporating fear effect in prey, Holling type IV functional response and specific mortality function on predator, the final model appears as follows:

$$\begin{aligned}\frac{dx}{dt} &= \frac{rx}{1+ky} - \beta x - \alpha x^2 - \frac{gxy}{1+hx^2}\,, \quad x(0) > 0\\ \frac{dy}{dt} &= \frac{mgxy}{1+hx^2} - \frac{(p+qy)}{1+y}y\,, \quad y(0) > 0\end{aligned} \tag{1}$$

Table 1: Descriptions of parameters

Parameter	Descriptions of Parameter
r	Birth rate of prey (> 0).
k	Level of fear due to predator.
β	Death rate of prey (> 0).
α	Decay rate for intraspecific competition.
g	Attack rate or predation rate of predator.
h	The decline rate in consumption at high prey densities.
m	Conversion factor ($0 < m < 1$).
p	Mortality rate of predator at low density.
q	Maximal mortality rate of predator.

Now we can rewrite the system of equations (1) as

$$\begin{aligned}\frac{dx}{dt} &= x\left(\frac{r}{1+ky} - \beta - \alpha x - \frac{gy}{1+hx^2}\right) \equiv F_1(x,y) = xf_1(x,y)\,, \quad x(0) > 0\\ \frac{dy}{dt} &= y\left(\frac{mgx}{1+hx^2} - \frac{(p+qy)}{1+y}\right) \equiv F_2(x,y) = yf_2(x,y)\,, \quad y(0) > 0\end{aligned} \tag{2}$$

where,

$$f_1(x,y) = \frac{r}{1+ky} - \beta - \alpha x - \frac{gy}{1+hx^2}$$

$$f_2(x,y) = \frac{mgx}{1+hx^2} - \frac{(p+qy)}{1+y}$$

3. Positivity and Boundedness

Theorem 3.1. *All the solutions of the system (2) that start in $\mathbb{R}^2_+$ remain positive for all time.*

Proof. Solving the system of equations (2) we get,

$$x(t) = x(0)\exp\left(\int_0^t f_1(x,y)dw\right) > 0, \text{ as } x(0) > 0,$$

$$y(t) = y(0)\exp\left(\int_0^t f_2(x,y)dw\right) > 0, \text{ as } y(0) > 0.$$

Thus, $x(t) > 0$ and $y(t) > 0$ for $t > 0$.
Therefore, all solutions that begin within the interior of the first octant remain positive for all time. □

Theorem 3.2. *Every solution of system (2) is uniformly bounded.*

Proof. In order to demonstrate the boundedness of the solution, let us assume the function $w(t) = x(t) + \frac{y(t)}{m}$. So we have,

$$\frac{dw}{dt} = \frac{dx}{dt} + \frac{1}{m}\frac{dy}{dt}$$
$$\Rightarrow \frac{dw}{dt} = \frac{rx}{1+ky} - \beta x - \alpha x^2 - \frac{(p+qy)}{m(1+y)}y$$
$$\Rightarrow \frac{dw}{dt} \leq \frac{rx}{1+ky} - \alpha x^2 - \mu\left[x + \frac{y}{m}\right] = \frac{rx}{1+ky} - \alpha x^2 - \mu w \qquad [\text{where, } \mu = \min\{\beta, p, q\}]$$
$$\Rightarrow \frac{dw}{dt} + \mu w \leq rx - \alpha x^2$$
$$\Rightarrow \frac{dw}{dt} + \mu w \leq -\alpha\left[x - \frac{r}{2\alpha}\right]^2 + \frac{r^2}{4\alpha}$$
$$\Rightarrow \frac{dw}{dt} + \mu w \leq \frac{r^2}{4\alpha} = M \text{ (say)}$$
$$\Rightarrow \frac{dw}{dt} + \mu w \leq M$$

Now by the principle of differential inequality [15], we get $0 < w(t) \leq \frac{M}{\mu}\left(1 - e^{-\mu t}\right) + w(0)e^{-\mu t}$. As $t \to \infty$, we get $0 < w(t) \leq \frac{M}{\mu} + \epsilon$, for any positive ϵ. Therefore, all solutions of system (2) eventually enter into the region: $B = \left\{(x, y) \in \mathbb{R}^2_+ : 0 < w(t) \leq \frac{M}{\mu} + \epsilon, \text{ for any positive } \epsilon\right\}$. Thus every solution of system (2) is uniformly bounded.

□

4. Equilibrium Points

4.1. Trivial and Axial equilibrium

System (2) always has $E_0(0, 0)$, $E_a(\frac{r-\beta}{\alpha}, 0)$ which indicate species free and predator free equilibrium point respectively. If death rate exceeds the intrinsic birth rate of any species, that species leads to an extinction, **so we assumed that,** $r > \beta$.

4.2. Interior Equilibrium

The interior equilibrium point of system (2) is determined by solving the two non-trivial nullclines, which are as follows:

$$f_1(x, y) = \frac{r}{1+ky} - \beta - \alpha x - \frac{gy}{1+hx^2} = 0 \tag{3}$$

$$f_2(x, y) = \frac{mgx}{1+hx^2} - \frac{(p+qy)}{1+y} = 0 \implies y = \frac{p(1+hx^2) - mgx}{mgx - q(1+hx^2)}. \tag{4}$$

Putting the value of y from (4) in (3), we get $\phi(x) = 0$, where

$\phi(x) = a_7x^7 + a_6x^6 + a_5x^5 + a_4x^4 + a_3x^3 + a_2x^2 + a_1x + a_0$
here,
$a_0 = (kp - q)(\beta q - pg) + q^2r$

$$a_1 = (kp - q)q\alpha + [2q(r - \beta) + (p + q)(k\beta - g) + 2pkg]$$

$$a_2 = 3(kp - q)hq\beta + [2q - (p + q)k]mg\alpha + 2(q^2r - p^2kg + pqg)h + [r + (1 - \beta)(1 - k)]m^2g^2$$

$$a_3 = 3(kp - q)hq\alpha + [4(r - \beta)q + 2pkg + (p + q)(2k\beta - g)]hmg - (1 - k)\alpha m^2g^2$$

$$a_4 = 3(kp - q)h^2q\beta + 2[2q - (p + q)k]hmg\alpha + (q^2r - p^2kg + pqg)h^2 + [r - (1 - k)]\beta hm^2g^2$$

$$a_5 = 3(kp - q)h^2q\alpha + [2q(r - \beta) + (p + q)k\beta]mgh^2 - (1 - k)\alpha m^2g^2h$$

$$a_6 = (kp - q)h^3q\beta + [2q - (p + q)k]h^2mg\alpha$$

$$a_7 = (kp - q)h^3q\alpha$$

If $kp < q < \dfrac{pg}{\beta}$, then $a_0 > 0$ and $a_7 < 0$. Thus Descartes's rule of sign [16], confirms at least one positive solution of $\phi(x) = 0$ say x^*. From (4) we have,

$$y^* = \frac{p(1 + hx^{*2}) - mgx^*}{mgx^* - q(1 + hx^{*2})} > 0\,, \qquad \text{provided,} \quad p < \frac{mgx^*}{(1 + hx^{*2})} < q.$$

There are some differences in the existence of system's interior equilibrium for an appropriate choice of parameters. We obtain several cases numerically, which are given below:

Case I: If $r = 1.5$, $k = 0.21$, $\beta = 0.13$, $\alpha = 0.25$, $g = 1.36$, $h = 0.44$, $m = 0.73$, $p = 0.32$ and $q = 1.15$, the non-trivial prey nullcline (green curve) and predator nullcline (red curve) do not intersect with each-other, which is shown in Figure 2a.

Case II: If $r = 1.75$, $k = 0.55$, $\beta = 0.38$, $\alpha = 0.35$, $g = 1.55$, $h = 0.52$, $m = 0.93$, $p = 0.47$, $q = 1.37$, the non-trivial prey nullcline (green curve) and predator nullcline (red curve) intersect at exactly one point say $E_{I1}(x_1^*, y_1^*)$, which is shown in Figure 2b.

Case III: If $r = 1.7$, $k = 0.46$, $\beta = 0.18$, $\alpha = 0.16$, $g = 1.49$, $h = 0.51$, $m = 0.93$, $p = 0.44$, $q = 1.24$, the non-trivial prey nullcline (green curve) and predator nullcline (red curve) intersect at two points say $E_{I1}(x_1^*, y_1^*)$ and $E_{I2}(x_2^*, y_2^*)$, which is shown in Figure 2c.

Case IV: If $r = 1.65$, $k = 0.5$, $\beta = 0.13$, $\alpha = 0.25$, $g = 1.02$, $h = 0.44$, $m = 0.98$, $p = 0.1$, $q = 1.15$, the non-trivial prey nullcline (green curve) and predator nullcline (red curve) intersect at three points say $E_{I1}(x_1^*, y_1^*)$, $E_{I2}(x_2^*, y_2^*)$ and $E_{I3}(x_3^*, y_3^*)$, which is shown in Figure 2d.

5. Stability Analysis

The Jacobian matrix of system (2) corresponding to the equilibrium point $E(x, y)$ is

$$J(x, y) = \begin{bmatrix} \dfrac{\partial F_1}{\partial x} & \dfrac{\partial F_1}{\partial y} \\ \dfrac{\partial F_2}{\partial x} & \dfrac{\partial F_2}{\partial y} \end{bmatrix}$$

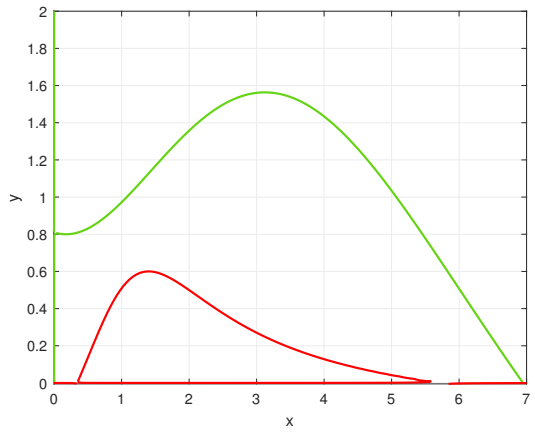

(a) There is no intersection between $f_1(x, y) = 0$ and $f_2(x, y) = 0$.

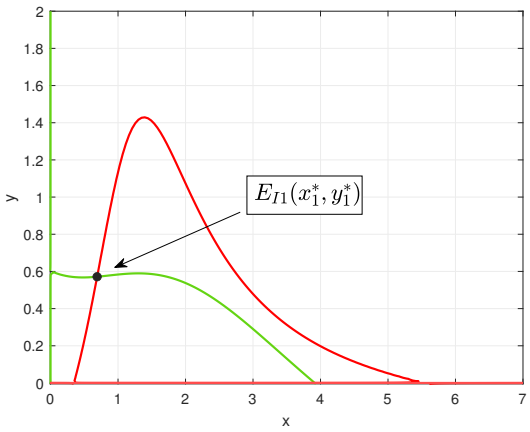

(b) The $f_1(x, y) = 0$ and $f_2(x, y) = 0$ intersect only at $E_{I1}(x_1^*, y_1^*)$.

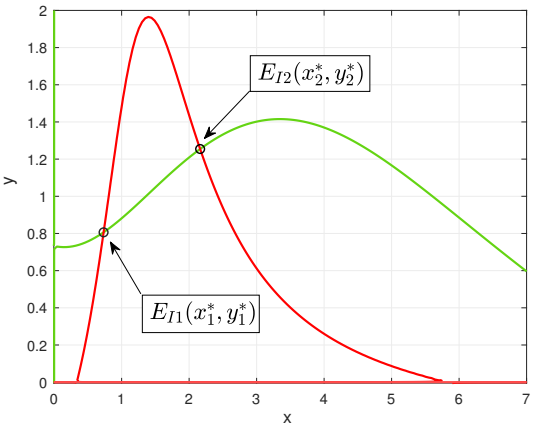

(c) $f_1(x, y) = 0$ and $f_2(x, y) = 0$ intersect at $E_{I1}(x_1^*, y_1^*)$ and $E_{I2}(x_2^*, y_2^*)$

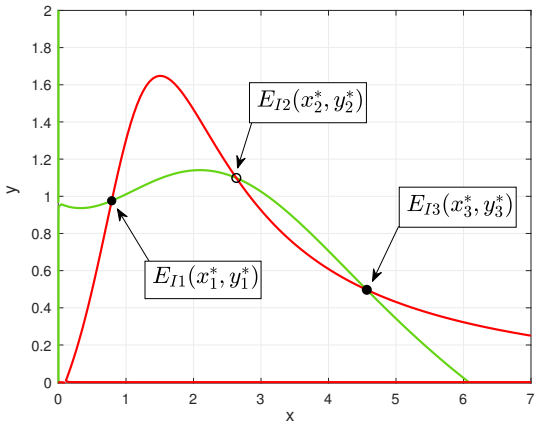

(d) $f_1(x, y) = 0$ and $f_2(x, y) = 0$ intersect at $E_{I1}(x_1^*, y_1^*)$, $E_{I2}(x_2^*, y_2^*)$ and $E_{I3}(x_3^*, y_3^*)$

Figure 2: Variation in the number of interior equilibrium points for a suitable choice of parameters. Here prey and predator nullcline are depicted by red and green curve respectively.

$$= \begin{bmatrix} \frac{r}{1+ky} - \beta - 2\alpha x - \frac{gy(1-hx^2)}{(1+hx^2)^2} & -\frac{rkx}{(1+ky)^2} - \frac{gx}{1+hx^2} \\ \frac{mgy(1-hx^2)}{(1+hx^2)^2} & \frac{mgx}{1+hx^2} - \frac{(p+2qy+qy^2)}{(1+y)^2} \end{bmatrix}$$

Theorem 5.1. *$E_0(0,0)$, the trivial equilibrium point of system (2) is always unstable.*

Proof. The Jacobian matrix $J(E_0(0,0))$ is given by

$$J(E_0) = \begin{bmatrix} r-\beta & 0 \\ 0 & -p \end{bmatrix}$$

The eigenvalues of $J(E_0)$ are $(r-\beta)$ and $-p$. Since it is biologically relevant to consider $r > \beta$, we have $(r-\beta) > 0$ and $-p < 0$. Therefore, $E_0(0,0)$ is a saddle point.

□

Theorem 5.2. *Predator-free equilibrium point $E_a(\frac{r-\beta}{\alpha}, 0)$ is locally asymptotically stable if $mg(\frac{r-\beta}{\alpha}) < p\left[1 + h(\frac{r-\beta}{\alpha})^2\right]$ and is an unstable saddle point if $mg(\frac{r-\beta}{\alpha}) > p\left[1 + h(\frac{r-\beta}{\alpha})^2\right]$.*

Proof. The Jacobian matrix $J(E_a)$ at $E_a = (\frac{r-\beta}{\alpha}, 0)$ is given by

$$J(E_a) = \begin{bmatrix} -(r-\beta) & -\frac{r-\beta}{\alpha}\left(rk + \frac{g\alpha^2}{\alpha^2 + h(r-\beta)^2}\right) \\ 0 & \frac{mg(\frac{r-\beta}{\alpha}) - p\left[1 + h(\frac{r-\beta}{\alpha})^2\right]}{1 + h(\frac{r-\beta}{\alpha})^2} \end{bmatrix}$$

The eigen values of $J(E_a)$ are $-(r-\beta)$ and $\frac{mg(\frac{r-\beta}{\alpha}) - p\left[1 + h(\frac{r-\beta}{\alpha})^2\right]}{1 + h(\frac{r-\beta}{\alpha})^2}$. Hence the predator free equilibrium is locally asymptotically stable if $mg\left(\frac{r-\beta}{\alpha}\right) < p\left[1 + h\left(\frac{r-\beta}{\alpha}\right)^2\right]$ and it is an unstable saddle if $mg\left(\frac{r-\beta}{\alpha}\right) > p\left[1 + h\left(\frac{r-\beta}{\alpha}\right)^2\right]$.

□

Theorem 5.3. *The coexistence equilibrium point $E_I(x^*, y^*)$ is locally asymptotically stable if $\mathcal{A}_1 > \mathcal{A}_2$ and $\mathcal{A}_3 < \mathcal{A}_4$.*
where, $\mathcal{A}_1 = \frac{mg}{(1+hx^{*2})^2}\left[\frac{rk}{(1+ky^*)^2} + \frac{g}{1+hx^{*2}}\right] + \frac{(q-p)\alpha}{(1+y^*)^2}$, $\mathcal{A}_3 = \frac{2ghx^{*2}y^*}{(1+hx^{*2})^2}$

$\mathcal{A}_2 = \frac{mghx^{*2}}{(1+hx^{*2})^2}\left[\frac{rk}{(1+ky^*)^2} + \frac{g}{1+hx^{*2}}\right] + \frac{2ghx^*y^*(q-p)}{(1+y^*)^2(1+hx^{*2})^2}$, $\mathcal{A}_4 = \alpha x^* + \frac{(q-p)y^*}{(1+y^*)^2}$

Proof. For the coexistence equilibrium point $E_I(x^*, y^*)$, the Jacobin matrix becomes,

$$J(E_I) = \begin{bmatrix} x\frac{\partial f_1}{\partial x} & x\frac{\partial f_1}{\partial y} \\ y\frac{\partial f_2}{\partial x} & y\frac{\partial f_2}{\partial y} \end{bmatrix}_{E_I} = \begin{bmatrix} J_{11} & J_{12} \\ J_{21} & J_{22} \end{bmatrix} = A$$

where,

$$J_{11} = -\alpha x^* + \frac{2ghx^{*2}y^*}{(1+hx^{*2})^2}\,,\ J_{12} = -\frac{rkx^*}{(1+ky^*)^2} - \frac{gx^*}{1+hx^{*2}}\,,\ J_{21} = \frac{(1-hx^{*2})mgy^*}{(1+hx^{*2})^2}\,,\ J_{22} = \frac{(p-q)y^*}{(1+y^*)^2}$$

Let, $\gamma = Tr(J(E_I)) = J_{11} + J_{22} = -\alpha x^* + \frac{2ghx^{*2}y^*}{(1+hx^{*2})^2} + \frac{(p-q)y^*}{(1+y^*)^2} = \mathcal{A}_3 - \mathcal{A}_4$

and $\delta = det(J(E_I)) = \left[xy\frac{\partial f_1}{\partial y}\frac{\partial f_2}{\partial y}\left(\frac{dy^{(f_2)}}{dx} - \frac{dy^{(f_1)}}{dx}\right)\right]_{E_I}$

$$= x^*y^*\left[\left(\frac{rk}{(1+ky^*)^2} + \frac{g}{1+hx^{*2}}\right)\frac{mg(1-hx^{*2})}{(1+hx^{*2})^2} - \frac{(q-p)}{(1+y^*)^2}\left(\frac{2ghx^*y^*}{(1+hx^{*2})^2} - \alpha\right)\right] = x^*y^*(\mathcal{A}_1 - \mathcal{A}_2)$$

where, $\mathcal{A}_1 = \frac{mg}{(1+hx^{*2})^2}\left[\frac{rk}{(1+ky^*)^2} + \frac{g}{1+hx^{*2}}\right] + \frac{(q-p)\alpha}{(1+y^*)^2}\,,\ \mathcal{A}_3 = \frac{2ghx^{*2}y^*}{(1+hx^{*2})^2}$

$$\mathcal{A}_2 = \frac{mghx^{*2}}{(1+hx^{*2})^2}\left[\frac{rk}{(1+ky^*)^2} + \frac{g}{1+hx^{*2}}\right] + \frac{2ghx^*y^*(q-p)}{(1+y^*)^2(1+hx^{*2})^2}\,,\ \mathcal{A}_4 = \alpha x^* + \frac{(q-p)y^*}{(1+y^*)^2}$$

So, when $\mathcal{A}_1 > \mathcal{A}_2$ and $\mathcal{A}_3 < \mathcal{A}_4$ the real part of the both eigen values are negative, hence the coexistence equilibrium point $E_I(x^*, y^*)$ is locally asymptotically stable. □

6. Bifurcation Analysis

6.1. Transcritical Bifurcation

Theorem 6.1. *The system (2) experiences a transcritical bifurcation around the predator-free equilibrium point* $E_a\left(\frac{r-\beta}{\alpha}, 0\right)$ *at the bifurcation threshold* $p^{(TC)} = \frac{mg\frac{(r-\beta)}{\alpha}}{1+h(\frac{r-\beta}{\alpha})^2}$.

Proof. Here we apply Sotomayor's theorem [17] to prove that the system (2) undergoes a transcritical bifurcation around $E_a\left(\frac{r-\beta}{\alpha}, 0\right)$ at the bifurcation threshold $p^{(TC)} = \frac{mg\frac{(r-\beta)}{\alpha}}{1+h(\frac{r-\beta}{\alpha})^2}$. Now the Jacobian matrix at E_a is

$$J(E_a) = \begin{bmatrix} -(r-\beta) & -\frac{r-\beta}{\alpha}\left(rk + \frac{g\alpha^2}{\alpha^2+h(r-\beta)^2}\right) \\ 0 & \frac{mg(\frac{r-\beta}{\alpha})}{1+h(\frac{r-\beta}{\alpha})^2} - p \end{bmatrix}$$

Now 0 is an eigen value of $J(E_a; p = p^{(TC)})$. The eigen vectors of $J(E_a; p = p^{(TC)})$ and $J(E_a; p = p^{(TC)})^t$ corresponding to the eigenvalue 0 are $V = \begin{pmatrix} v_1 \\ 1 \end{pmatrix}$ and $W = \begin{pmatrix} 0 \\ 1 \end{pmatrix}$ respectively,

where $v_1 = -\frac{1}{\alpha}\left(rk + \frac{g\alpha^2}{r^2+h(r-\beta)^2}\right)$. The transversality conditions for transcritical bifurcation are

$$\Delta_1 = W^t\left[F_p\left(E_a; p = p^{(TC)}\right)\right] = 0,$$

$$\Delta_2 = W^t\left[DF_p\left(E_a; p = p^{(TC)}\right)V\right] = -1 \neq 0,$$

$$\Delta_3 = W^t\left[D^2F\left(E_a; p = p^{(TC)}\right)(V,V)\right] \neq 0\,, \qquad \text{provided, } q + \frac{A_1h(r-\beta)^2}{\alpha^2} \neq A_1 + \frac{mg\frac{(r-\beta)}{\alpha}}{1+h(\frac{r-\beta}{\alpha})^2}$$

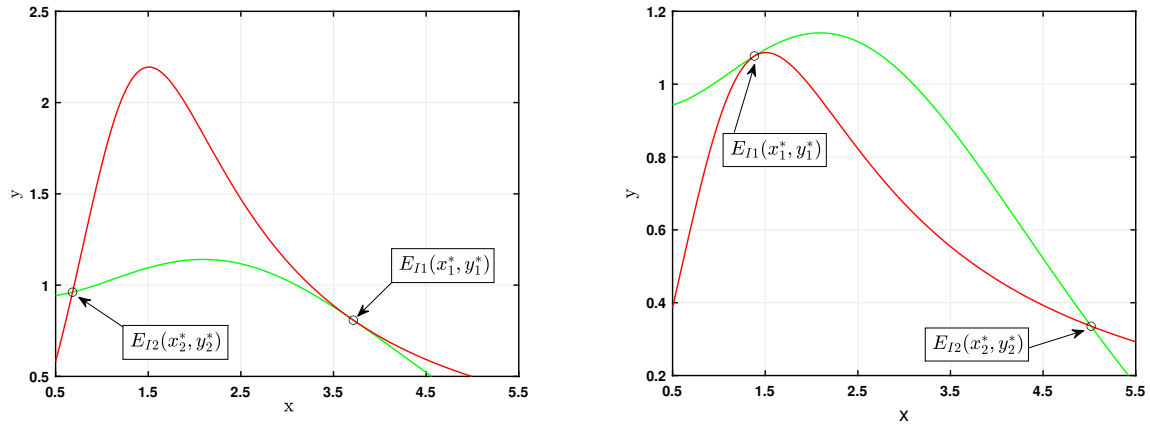

(a) $q = 1.0512027$ (b) $q = 1.3547206$

Figure 3: Occurrence of the saddle-node bifurcations for the non-trivial prey nullclines (green curve) and predator nullclines (red curve).

where, $A_1 = \dfrac{gm\left(\frac{\alpha^2 q}{h(r-\beta)^2+r^2} + kr\right)}{\alpha\left(\frac{h(r-\beta)^2}{\alpha^2} + 1\right)}$.

Here, $F \equiv \begin{pmatrix} F_1 \\ F_2 \end{pmatrix}$, F_1 and F_2 are defined in the system (2). So, by Sotomayor's theorem, the system experiences a transcritical bifurcation around $E_a\left(\dfrac{r-\beta}{\alpha}, 0\right)$ at the bifurcation threshold $p^{(TC)} = \dfrac{mg\frac{(r-\beta)}{\alpha}}{1 + h(\frac{r-\beta}{\alpha})^2}$. □

Remark: The system (2) undergoes a transcritical bifurcation with respect to the bifurcation parameter r.

6.2. *Saddle–node bifurcation*

A saddle-node bifurcation arises when two equilibrium points within the system converge, collide, and vanish as a result of the parameter's variation, leading to their mutual annihilation. Here q, the maximal mortality of predator is considered as the bifurcation parameter. The saddle-node bifurcation appears when the predator and prey nullclines touch tangentially. Figure 3 shows that non-trivial prey and predator nullclines touches each other for two different values of q, namely $q^{(SN_1)}$ and $q^{(SN_2)}$ and setting the remaining parameter values at $\{r = 1.65, k = 0.5, \beta = 0.13, \alpha = 0.25, g = 1.02, h = 0.44, m = 0.98, p = 0.1\}$.

Now we will provide a theorem that proves the occurrence of a saddle-node bifurcation in the system with respect to the bifurcation parameter q.

Theorem 6.2. *The system (2) experiences a saddle-node bifurcation with respect to the bifurcation parameter q.*

Proof. Let, $\Phi(x) \equiv a_7x^7 + a_6x^6 + a_5x^5 + a_4x^4 + a_3x^3 + a_2x^2 + a_1x + a_0 = 0$ has a root of multiplicity two for a certain critical value of q, say x^*. Geometrically, this occurs when the non trivial prey nullcline $(f_1(x, y) = 0)$ intersects the predator nullcline $(f_2(x, y) = 0)$ at a point of tangency $(E_{I1}(x_1^*, y_1^*))$. Then the slope of two nullcline are equal so,

$$\left.\frac{dy^{(f_1)}}{dx}\right|_{E_{I1}} = \left.\frac{dy^{(f_2)}}{dx}\right|_{E_{I1}}.$$

The Jacobian matrix $J(E_{I1})$ at $q = q^{(SN_1)}$ is given by ,

$$J(E_{I1}; q = q^{(SN_1)}) = \begin{bmatrix} x\frac{\partial f_1}{\partial x} & x\frac{\partial f_1}{\partial y} \\ y\frac{\partial f_2}{\partial x} & y\frac{\partial f_2}{\partial y} \end{bmatrix}_{E_{I1}, q^{(SN_1)}}$$

$$= \begin{bmatrix} x\left(-\alpha + \frac{2ghxy}{(1+hx^2)^2}\right) & -\frac{rkx}{(1+ky)^2} - \frac{gx}{1+hx^2} \\ mgy\left(\frac{1-hx^2}{(1+hx^2)^2}\right) & \frac{(p-q)y}{(1+y)^2} \end{bmatrix}_{E_{I1}, q^{(SN_1)}}$$

Now,

$$det(J(E_{I1}; q = q^{(SN_1)})) = \left[xy\left(\frac{\partial f_1}{\partial x}\frac{\partial f_2}{\partial y} - \frac{\partial f_1}{\partial y}\frac{\partial f_2}{\partial x}\right)\right]_{E_{I1}, q^{(SN_1)}} = \left[xy\frac{\partial f_1}{\partial y}\frac{\partial f_2}{\partial y}\left(\frac{dy^{(f_2)}}{dx} - \frac{dy^{(f_1)}}{dx}\right)\right]_{E_{I1}, q^{(SN_1)}} = 0.$$

Hence, $J(E_{I1}; q = q^{(SN_1)})$ has zero eigen-value. Now the eigen vectors corresponding to the zero eigen-value of $J(E_{I1}; q = q^{(SN_1)})$ and $\left[J(E_{I1}; q = q^{(SN_1)})\right]^t$ are $V = \begin{pmatrix} 1 \\ v_1 \end{pmatrix}_{E_{I1}, q^{(SN_1)}}$ and $W = \begin{pmatrix} 1 \\ w_1 \end{pmatrix}_{E_{I1}, q^{(SN_1)}}$ respectively, where $v_1 = \frac{mg(1+y)^2(1-hx^2)}{(q-p)(1+hx^2)^2}$ and $w_1 = -\frac{(1+y)^2 x}{(q-p)y}\left[\frac{rk}{(1+ky)^2} + \frac{g}{(1+hx^2)}\right]$. The transversality conditions for saddle–node bifurcation are :

$$W^t\left[F_q(E_{I1}; q = q^{(SN_1)})\right] = \left[\frac{(1+y_1^*)^2 x_1^*}{(q-p)(1+y_1^{*2})}\left(\frac{rk}{(1+ky_1^*)^2} + \frac{g}{(1+hx_1^{*2})}\right)\right]_{q=q^{(SN_1)}} \neq 0,$$

$$W^t\left[D^2F(E_{I1}; q = q^{(SN_1)})(V, V)\right] = 2\alpha - R \neq 0, \qquad \text{provided, } 2\alpha \neq R$$

where, $R = \frac{2ghx_1^* y_1^*(3 - hx_1^{*2})}{(1+hx_1^{*2})^3}\left[1 + \frac{(1+y_1^*)^2 m x_1^*}{(q^{(SN_1)} - p)}\left(\frac{rk}{(1+ky_1^*)^2} + \frac{g}{1+hx_1^{*2}}\right)\right]$
$- \frac{2mg(1+y_1^*)^2(1-hx_1^{*2})}{(q^{(SN_1)} - p)(1+hx_1^{*2})}\left[\frac{rk}{(1+ky_1^*)^2} + \frac{g(1-hx_1^{*2})}{(1+hx_1^{*2})^2}\left[1 + \frac{(1+y_1^*)^2 m x_1^*}{(q^{(SN_1)} - p)}\left(\frac{rk}{(1+ky_1^*)^2} + \frac{g}{1+hx_1^{*2}}\right)\right]\right]$
$+ \frac{m^2 g^2 (1+y_1^*)^4 (1-hx_1^{*2})^2}{(q^{(SN_1)} - p)^2 (1+hx_1^{*2})^2}\left[\frac{2r^2 k x_1^*}{(1+ky_1^*)^3} + \frac{2x_1^*}{y_1^*(1+y_1^*)}\left(\frac{rk}{(1+ky_1^*)^2} + \frac{g}{1+hx_1^{*2}}\right)\right]$

Therefore, according to Sotomayor's theorem [17], it is concluded that the system undergoes a saddle-node bifurcation around the interior equilibrium point $E_{I1}(x_1^*, y_1^*)$ at $q = q^{(SN_1)}$. Similarly, another saddle-node bifurcation occurs at the interior equilibrium point $E_{I2}(x_2^*, y_2^*)$ when $q = q^{(SN_2)}$. □

Remark: The system (2) undergoes a saddle-node bifurcation with respect to the bifurcation parameters p, k and r.

6.3. Hopf bifurcation

Taking k, the fear level as a changing parameter the characteristic equation of the Jacobian matrix $J(E_I)$ can be written as

$$\lambda^2 - \gamma(k)\lambda + \delta(k) = 0 \tag{5}$$

where the smooth functions $\delta(k)$ and $\gamma(k)$ are the determinant and trace of $J(E_I)$, explicitly defined in the proof of theorem (5.3). Here, the sign of the real parts of the eigen values λ determine the stability of $E_I(x^*, y^*)$. For negative real parts, E_I is stable and for positive real part, E_I is unstable. Thus, the shift in stability happens when the characteristic equation (5) possesses purely imaginary roots. Let us assume at $k = k^{(H)}$,$\gamma(k^{(H)}) = 0$ and $\delta(k^{(H)}) > 0$, i.e., the roots of (5) are purely imaginary at $k = k^{(H)}$. Next, we will prove in the following theorem that the Hopf bifurcation occurs in system (2) at $k = k^{(H)}$.

Theorem 6.3. *For the bifurcation parameter k, system (2) undergoes a Hopf bifurcation around $E_I(x^*, y^*)$ at $k = k^{(H)}$ provided $\gamma(k^{(H)}) = 0$, $\delta(k^{(H)}) > 0$ and* $\left[\frac{d\gamma}{dk}\right]_{k^{(H)}} \neq 0$.

Proof. The characteristic equation (5) has two purely imaginary roots $\lambda_1 = i\sqrt{\delta(k^{(H)})}$ and $\lambda_2 = -i\sqrt{\delta(k^{(H)})}$ at $k = k^{(H)}$ as, $\gamma(k^{(H)}) = 0$ and $\delta(k^{(H)}) > 0$. Therefore characteristic roots of the equation (5) is of the form $\lambda_1(k) = p_1(k) + ip_2(k)$ and $\lambda_2(k) = p_1(k) - ip_2(k)$ in an open neighbourhood of $k^{(H)}$ where $p_1(k)$ and $p_2(k)$ are real valued functions of k. So, the system changes its stability if the transvarsality condition of Hopf-Bifurcation Theorem [18],

$$\left[\frac{d}{dk}(Re(\lambda_i(k)))\right]_{k=k^{(H)}} = \left[\frac{d}{dk}(p_1(k))\right]_{k=k^{(H)}} \neq 0$$

is satisfied. Substituting $\lambda(k) = p_1(k) + ip_2(k)$ in (5) and differentiating w.r.t. k, we get

$$2\Big(p_1(k) + ip_2(k)\Big)\Big(\dot{p}_1(k) + i\dot{p}_2(k)\Big) - \gamma(k)\Big(\dot{p}_1(k) + i\dot{p}_2(k)\Big) - \dot{\gamma}(k)\Big(p_1(k) + ip_2(k)\Big) + \dot{\delta}(k) = 0$$

Comparing the real and complex parts, we have

$$\dot{p}_1(2p_1 - \gamma) + \dot{p}_2(-2p_2) - \dot{\gamma}p_1 + \dot{\delta} = 0 \implies \dot{p}_1X_1 - \dot{p}_2X_2 + X_3 = 0;$$

$$\dot{p}_1(2p_2) + \dot{p}_2(2p_1 - \gamma) - \dot{\gamma}p_2 = 0 \implies \dot{p}_1X_2 + \dot{p}_2X_1 + X_4 = 0;$$

where, $X_1 = (2p_1 - \gamma)$, $X_2 = 2p_2$, $X_3 = (-\dot{\gamma}p_1 + \dot{\delta})$ and $X_4 = -\dot{\gamma}p_2$

Solving the above system we get,

$$\dot{p}_1 = -\frac{(X_1X_3 + X_2X_4)}{X_1^2 + X_2^2} \tag{6}$$

Now, for $k = k^{(H)}$ i.e. for $p_1(k) = 0$, two cases arise:

Case I: $p_2 = \sqrt{\delta}$. Therefore $X_1 = 0$, $X_2 = 2\sqrt{\delta}$, $X_3 = \dot{\delta}$ and $X_4 = -\dot{\gamma}\sqrt{\delta}$. Hence from (6) we get

$$\left[\frac{d}{dk}(p_1(k))\right]_{k=k^{(H)}} = \frac{1}{2}\left[\frac{d}{dk}(\gamma(k))\right]_{k=k^{(H)}} \neq 0\,, \qquad \text{provided, } k^{(H)} \neq \frac{1}{y^*}$$

Case II: $p_2 = -\sqrt{\delta}$. Therefore $X_1 = 0$, $X_2 = -2\sqrt{\delta}$, $X_3 = \dot{\delta}$ and $X_4 = \dot{\gamma}\sqrt{\delta}$. So from (6) we get

$$\left[\frac{d}{dk}(p_1(k))\right]_{k=k^{(H)}} = \frac{1}{2}\left[\frac{d}{dk}(\gamma(k))\right]_{k=k^{(H)}} \neq 0\,, \qquad \text{provided, } k^{(H)} \neq \frac{1}{y^*}$$

Hence proved. □

Remark: For the bifurcation parameter r, system (2) undergoes a Hopf bifurcation around the interior equilibrium $E_I(x^*, y^*)$

6.4. Cusp bifurcation

It has been observed that the system (2) possesses three coexistence equilibrium points for a suitable choice of parametric values say, $E_{I1}({x_1}^*, {y_1}^*)$, $E_{I2}({x_2}^*, {y_2}^*)$ and $E_{I3}({x_3}^*, {y_3}^*)$. Now, for a continuous change of a parametric value, two cases appear: either E_{I1} coincides with E_{I2} or E_{I2} coincides with E_{I3} at a point, leads to the occurrence of two saddle-node bifurcation curve. If these two branches of saddle-node bifurcation curve meet tangentially at a point, the cusp bifurcation emerges. That is, three interior equilibrium points coincide together at this cusp point. Therefore the system (2) experiences a cusp bifurcation.

6.5. Bogdanov-Takens bifurcation

The system (2) undergoes both saddle-node bifurcation and Hopf-bifurcation for a proper set of parametric values, resulting in a saddle-node bifurcation curve and a Hopf bifurcation curve within a specific two-parameter bifurcation plane. When the Hopf-bifurcation curve intersects saddle-node bifurcation curve, a new bifurcation known as the Bogdanov-Takens bifurcation emerges. Usually, a Bogdanov-Takens (BT) bifurcation refers to a point, in which the Jacobian matrix has a zero eigenvalue with algebraic multiplicity two. Now we will provide a theorem that proves the occurrence of a Bogdanov–Takens bifurcation in the system with respect to the bifurcation parameters q and r.

Theorem 6.4. *The system (2) undergoes a Bogdanov–Takens bifurcation around the interior equilibrium point $E_I(x^*, y^*)$ with respect to the bifurcation parameters q, r, whenever satisfies the following conditions:*
(BT1) $tr(J(E_I; (q_{BT}, r_{BT}))) = 0$
(BT2) $det(J(E_I; (q_{BT}, r_{BT}))) = 0$

Proof. Conditions (BT1) and (BT2) are equivalent to following

$$x^*\Big(-\alpha + \frac{2ghx^*y^*}{(1+hx^{*2})^2}\Big) + \frac{(p-q_{BT})y^*}{(1+y^*)^2} = 0$$
$$x^*\Big(-\alpha + \frac{2ghx^*y^*}{(1+hx^{*2})^2}\Big)\frac{(p-q_{BT})y^*}{(1+y^*)^2} + \Big[\frac{r_{BT}kx^*}{(1+ky^*)^2} + \frac{gx^*}{1+hx^{*2}}\Big]\Big(\frac{1-hx^{*2}}{(1+hx^{*2})^2}\Big)mgy^* = 0$$

From above expressions we can write explicitly

$$q_{BT} = p - \frac{x^*(1+y^*)^2}{y^*}\Big[\alpha - \frac{2ghx^*y^*}{(1+hx^{*2})^2}\Big],$$
$$r_{BT} = \Big[\frac{x^*(1+hx^{*2})^2(1+ky^*)^2}{kmgy^*(1-hx^{*2})}\Big]\Big(\alpha - \frac{2ghx^*y^*}{(1+hx^{*2})^2}\Big)^2 - \frac{g(1+ky^*)^2}{k(1+hx^{*2})}$$

Let us consider a small perturbation around the bifurcation threshold (q_{BT}, r_{BT}) say $(q_{BT} + \lambda_2, r_{BT} + \lambda_1)$, where $\{\lambda_i; i = 1, 2\}$ are sufficiently small.
Then system (2) becomes

$$\begin{aligned}
\frac{dx}{dt} &= \frac{(r+\lambda_1)x}{1+ky} - \beta x - \alpha x^2 - \frac{gxy}{1+hx^2} \equiv G_1(x, y, \lambda_1) = F_1(x, y) + \frac{\lambda_1 x}{1+ky} \\
\frac{dy}{dt} &= \frac{mgxy}{1+hx^2} - \frac{\big[p + (q+\lambda_2)y\big]y}{1+y} \equiv G_2(x, y, \lambda_2) = F_2(x, y) - \frac{\lambda_2 y^2}{1+y}
\end{aligned} \tag{7}$$

Now we shift the equilibrium point $E_I(x^*, y^*)$ to the origin by the transformations $x_1 = x - x^*$ and $x_2 = y - y^*$. So system (7) becomes

$$\begin{aligned}
\frac{dx_1}{dt} &= p_{00} + p_{10}x_1 + p_{01}x_2 + \frac{p_{11}}{2}{x_1}^2 + p_{12}x_1x_2 + \frac{p_{22}}{2}{x_2}^2 + \dots \\
\frac{dx_2}{dt} &= q_{00} + q_{10}x_1 + q_{01}x_2 + \frac{q_{11}}{2}{x_1}^2 + q_{12}x_1x_2 + \frac{q_{22}}{2}{x_2}^2 + \dots
\end{aligned} \tag{8}$$

where,

$$p_{00} = G_1(x^*, y^*, \lambda_1)\ ,\ q_{00} = G_2(x^*, y^*, \lambda_2)\ ,\ p_{10} = \frac{\partial G_1}{\partial x}(x^*, y^*, \lambda_1) = a + \frac{\lambda_1}{1+ky^*}$$

$$q_{10} = \frac{\partial G_2}{\partial x}(x^*, y^*, \lambda_2) = c\ ,\ p_{01} = \frac{\partial G_1}{\partial y}(x^*, y^*, \lambda_1) = b - \frac{\lambda_1 k x^*}{(1+ky^*)^2}$$

$$q_{01} = \frac{\partial G_2}{\partial y}(x^*, y^*, \lambda_2) = d - \frac{(2y^* + y^{*2})\lambda_2}{(1+y^*)^2}\ ,\ p_{11} = \frac{\partial^2 G_1}{\partial x^2}(x^*, y^*, \lambda_1) = \frac{2ghx^*y^*(3-hx^{*2})}{(1+hx^{*2})^3} - 2\alpha$$

$$q_{11} = \frac{\partial^2 G_2}{\partial x^2}(x^*, y^*, \lambda_2) = \frac{2hmgx^*y^*(hx^{*2}-3)}{(1+hx^{*2})^3}\ ,\ p_{12} = \frac{\partial^2 G_1}{\partial y \partial x}(x^*, y^*, \lambda_1) = -\frac{g(1-hx^{*2})}{(1+hx^{*2})^2} - \frac{k(r+\lambda_1)}{(1+ky^*)^2}$$

$$q_{12} = \frac{\partial^2 G_2}{\partial y \partial x}(x^*, y^*, \lambda_2) = \frac{mg(1-hx^{*2})}{(1+hx^{*2})^2}\ ,\ p_{22} = \frac{\partial^2 G_1}{\partial y^2}(x^*, y^*, \lambda_1) = \frac{2k^2x^*(r+\lambda_1)}{(1+ky^*)^3}$$

$$q_{22} = \frac{\partial^2 G_2}{\partial y^2}(x^*, y^*, \lambda_2) = \frac{2(p-q-\lambda_2)}{(1+y^*)^3}$$

Here, $a = -\alpha x^* + \frac{2ghx^{*2}y^*}{(1+hx^{*2})^2}$, $b = -\frac{rkx^*}{(1+ky^*)^2} - \frac{gx^*}{1+hx^{*2}}$, $c = \frac{(1-hx^{*2})mgy^*}{(1+hx^{*2})^2}$, $d = \frac{(p-q)y^*}{(1+y^*)^2}$.

Now, introducing affine transformation [17] $z_1 = x_1$, $z_2 = ax_1 + bx_2$, then the above system is transformed into

$$\begin{aligned}
\frac{dz_1}{dt} &= z_2 + \zeta_{00}(\lambda) + \zeta_{10}(\lambda)z_1 + \zeta_{01}(\lambda)z_2 + \frac{\zeta_{20}(\lambda)}{2}{z_1}^2 + \zeta_{11}z_1z_2 + \frac{\zeta_{02}(\lambda)}{2}{z_2}^2 + B_1(z_1, z_2)\\
\frac{dz_2}{dt} &= \eta_{00}(\lambda) + \eta_{10}(\lambda)z_1 + \eta_{01}(\lambda)z_2 + \frac{\eta_{20}(\lambda)}{2}{z_1}^2 + \eta_{11}z_1z_2 + \frac{\eta_{02}}{2}{z_2}^2 + B_2(z_1, z_2)
\end{aligned} \tag{9}$$

where, $\lambda = (\lambda_1, \lambda_2)$ and

$$\zeta_{00}(\lambda) = G_1(x^*, y^*, \lambda)\ ,\ \eta_{00}(\lambda) = aG_1(x^*, y^*, \lambda) + bG_2(x^*, y^*, \lambda)\ ,\ \zeta_{10}(\lambda) = (p_{10} - \frac{a}{b}p_{01})$$

$$\eta_{10}(\lambda) = bq_{10} - aq_{01} + ap_{10} - \frac{a^2}{b}p_{01}\ ,\ \zeta_{01}(\lambda) = \frac{1}{b}p_{01} - 1\ ,\ \eta_{01}(\lambda) = q_{01} + \frac{a}{b}p_{01}\ ,\ \zeta_{20}(\lambda) = \Big[p_{11} - \frac{2ap_{12}}{b} + \frac{a^2p_{22}}{b^2}\Big]$$

$$\eta_{20}(\lambda) = \Big[ap_{11} + bq_{11} - \frac{2a(ap_{12}+bq_{12})}{b} + \frac{a^2(ap_{22}+bq_{22})}{b^2}\Big]\ ,\ \zeta_{11}(\lambda) = \Big[\frac{p_{12}}{b} - \frac{ap_{22}}{b^2}\Big]$$

$$\eta_{11}(\lambda) = \Big[\frac{(ap_{12}+bq_{12})}{b} - \frac{a(ap_{22}+bq_{22})}{b^2}\Big]\ ,\ \zeta_{02}(\lambda) = \frac{p_{22}}{b^2}\ ,\ \eta_{02}(\lambda) = \frac{(ap_{22}+bq_{22})}{b^2}$$

The degeneracy conditions [19] of the Bogdanov-Takens bifurcations at (q_{BT}, r_{BT}) are,

I. $\begin{bmatrix} a & b \\ c & d \end{bmatrix} \neq \begin{bmatrix} 0 & 0 \\ 0 & 0 \end{bmatrix}$

II. $\zeta_{20}(0) + \eta_{11}(0) = R_1 - 2\alpha \neq 0$ provided, $2\alpha \neq R_1$

where, $R_1 = \dfrac{gm\left(1-hx^{*2}\right)\left(\alpha\left(y^*-1\right)\left(hx^{*2}+1\right)^2 - 4ghx^*y^{*2}\right)}{\left(y^*+1\right)\left(hx^{*2}+1\right)^2\left(\alpha\left(hx^{*2}+1\right)^2 - 2ghx^*y^*\right)} + \dfrac{\alpha\left(hx^{*2}+1\right)^2 - 4ghx^*y^*\left(hx^{*2}-1\right)}{\left(hx^{*2}+1\right)^3}$

Also,

III. $\eta_{20} = \left(\alpha - \dfrac{2ghx^*y^*}{\left(hx^{*2}+1\right)^2}\right)\left(2\alpha x^* + \dfrac{2ghx^{*2}y^*\left(hx^{*2}-3\right)}{\left(hx^{*2}+1\right)^3}\right) + \dfrac{2hx^{*3}\left(hx^{*2}-3\right)\left(\alpha - \dfrac{2ghx^*y^*}{\left(hx^{*2}+1\right)^2}\right)^2}{\left(hx^{*2}+1\right)\left(1-hx^{*2}\right)}$

$$+\frac{2gmy^*\left(1-hx^{*2}\right)}{\left(hx^{*2}+1\right)^2}\left(\frac{2ghx^{*2}}{\left(hx^{*2}+1\right)^2}-\frac{x^*\left(hx^{*2}+1\right)^2}{gmy^*\left(1-hx^{*2}\right)}\left(\alpha-\frac{2ghx^*y^*}{\left(hx^{*2}+1\right)^2}\right)^2\right)-\frac{x^*}{y^*}\left(\alpha-\frac{2ghx^*y^*}{\left(hx^{*2}+1\right)^2}\right)$$
$$+\frac{\left(gmy^*\left(1-hx^{*2}\right)\right)^2}{\left(hx^{*2}+1\right)^2\left(\alpha\left(hx^{*2}+1\right)^2-2ghx^*y^*\right)}\left(\frac{2x^*\left(ky^{*2}-1\right)\left(\alpha\left(hx^{*2}+1\right)^2-2ghx^*y^*\right)^2}{gmy^{*2}\left(y^*+1\right)\left(1-hx^{*2}\right)\left(hx^{*2}+1\right)^2\left(ky^*+1\right)}-\right.$$
$$\left.\frac{2gk}{\left(hx^{*2}+1\right)\left(ky^*+1\right)}\right)$$

Therefore, $\zeta_{20}(0)+\eta_{11}(0)\neq 0$ and $\eta_{20}(0)$ may or may not be 0. So, when $\eta_{20}(0)\neq 0$, then according to **sign** $[\eta_{20}(0)(\zeta_{20}(0)+\eta_{11}(0))]$, i.e., either +1 or −1, the predator-prey model undergoes a subcritical BT bifurcation or undergoes a supercritical BT bifurcation respectively. It is difficult to show that $\eta_{20}(0)\neq 0$ but we can assure the existence of Bogdanov-Takens bifurcation numerically for certain choice of parameters shown in Section 7. □

Remark: Also the system (2) undergoes Bogdanov–Takens bifurcation around an interior equilibrium point $E_I(x^*, y^*)$ for the pair of parameters $\{q, p\}$ and $\{p, r\}$.

6.6. Generalized Hopf bifurcation

The stability of the interior equilibrium point can be modified by supercritical or subcritical Hopf bifurcations, with the bifurcation type determined by the first Lyapunov coefficient (σ). A supercritical Hopf bifurcation leads to a stable limit cycle, characterized by $\sigma<0$, while a subcritical Hopf bifurcation results in an unstable limit cycle, characterized by ($\sigma>0$). The system undergoes a generalized Hopf bifurcation at ($\sigma=0$), which separates the two types of Hopf bifurcations. Now we will provide a theorem that proves the occurrence of a Generalized Hopf bifurcation in the system with respect to the bifurcation parameters p and r.

Theorem 6.5. *The system (2) experiences a Bautin (Generalized Hopf) bifurcation at the interior equilibrium point $E_I(x^*, y^*)$ around the bifurcation threshold (p_{GH}, r_{GH}) whenever $E_I(x^*, y^*)$ satisfies the following conditions:*
(GH1) $T = tr(J(E_I;(p_{GH}, r_{GH}))) = 0$
(GH2) $D = det(J(E_I;(p_{GH}, r_{GH}))) > 0$
(GH3) $L(E_I;(p_{GH}, r_{GH})) = 0$
where L is the first lyapunov number.

Proof. Let the nontrivial equilibrium point $E_I(x^*, y^*)$ satisfies the above three conditions. The Jacobian matrix at E_I is

$$J(E_I)=\begin{bmatrix} x\frac{\partial f_1}{\partial x} & x\frac{\partial f_1}{\partial y} \\ y\frac{\partial f_2}{\partial x} & y\frac{\partial f_2}{\partial y}\end{bmatrix}_{E_I}=\begin{bmatrix} x^*\left(-\alpha+\frac{2ghx^*y^*}{(1+hx^{*2})^2}\right) & -\frac{rkx^*}{(1+ky^*)^2}-\frac{gx^*}{1+hx^{*2}} \\ mgy^*\left(\frac{1-hx^{*2}}{(1+hx^{*2})^2}\right) & \frac{(p-q)y^*}{(1+y^*)^2}\end{bmatrix}$$

Now, from the condition ($GH1$) and ($GH2$):

$$p_{GH}=q+\frac{x^*(1+y^*)^2}{y^*}\left[\alpha-\frac{2ghx^*y^*}{(1+hx^{*2})^2}\right].$$

To find the first lyapunov number L at E_I we translate E_I to origin by using the transformation $x_1=x-x^*$

and $x_2 = y - y^*$. So, the system (2) becomes

$$\frac{dx_1}{dt} = ax_1 + bx_2 + P(x_1, x_2)$$
$$\frac{dx_2}{dt} = cx_1 + dx_2 + Q(x_1, x_2)$$

where, $a = \left(\frac{\partial F_1}{\partial x}\right)_{E_I}$, $b = \left(\frac{\partial F_1}{\partial y}\right)_{E_I}$, $c = \left(\frac{\partial F_2}{\partial x}\right)_{E_I}$, $d = \left(\frac{\partial F_2}{\partial y}\right)_{E_I}$ and $P(x_1, x_2)$, $Q(x_1, x_2)$ are analytic functions, defined by

$$P(x_1, x_2) = \sum_{i+j\geq 2} a_{ij} {x_1}^i {x_2}^j$$
$$Q(x_1, x_2) = \sum_{i+j\geq 2} b_{ij} {x_1}^i {x_2}^j$$

where, a_{ij} and b_{ij} are defined by, $a_{ij} = \frac{1}{i!\ j!}\left(\frac{\partial^{i+j} F_1}{\partial x^i \partial y^j}\right)_{E_I}$ and $b_{ij} = \frac{1}{i!\ j!}\left(\frac{\partial^{i+j} F_2}{\partial x^i \partial y^j}\right)_{E_I}$

Now, the first Lyapunov number [19] is as follows;

$$L = -\frac{3\pi}{2bD^{\frac{3}{2}}}\Big[\Big\{ac(a_{11}^2 + a_{11}b_{02} + a_{02}b_{11}) + ab(b_{11}^2 + a_{20}b_{11} + a_{11}b_{02}) + c^2(a_{11}a_{02} + 2a_{02}b_{02}) - 2ac(b_{02}^2 - a_{20}a_{02}) - 2ab(a_{20}^2 - b_{20}b_{02}) - b^2(2a_{20}b_{20} + b_{11}b_{20}) + (bc - 2a^2)(b_{11}b_{02} - a_{11}a_{20})\Big\} - (a^2 + bc)\Big\{3(cb_{03} - ba_{30}) + 2a(a_{21} + b_{12}) + (ca_{12} - bb_{21})\Big\}\Big]$$

Let us determine the coefficients a_{ij}, b_{ij} and a, b, c and d to calculate the first Lyapunov number.

$$a = \frac{\partial F_1}{\partial x}(x^*, y^*) = -\alpha x^* + \frac{2ghx^{*2}y^*}{(1 + hx^{*2})^2}\ ,\ b = \frac{\partial F_1}{\partial y}(x^*, y^*) = -\frac{rkx^*}{(1 + ky^*)^2} - \frac{gx^*}{1 + hx^{*2}}$$
$$c = \frac{\partial F_2}{\partial x}(x^*, y^*) = \frac{mgy^*(1 - hx^{*2})}{(1 + hx^{*2})^2}\ ,\ d = \frac{\partial F_2}{\partial y}(x^*, y^*) = \frac{(p - q)y^*}{(1 + y^*)^2}\ , D = det\,(J(E_I))$$
$$a_{11} = \frac{\partial^2 F_1}{\partial y \partial x}(x^*, y^*) = -\frac{g(1 - hx^{*2})}{(1 + hx^{*2})^2} - \frac{rk}{(1 + ky^*)^2}\ ,\ b_{03} = \frac{1}{6}\frac{\partial^3 F_2}{\partial y^3}(x^*, y^*) = \frac{(q - p)}{(1 + y^*)^4}$$
$$a_{20} = \frac{1}{2}\frac{\partial^2 F_1}{\partial x^2}(x^*, y^*) = \frac{ghx^*y^*(1 - 3hx^{*2})}{(1 + hx^{*2})^3} + \frac{2ghx^*y^*}{(1 + hx^{*2})^2} - \alpha\ ,\ a_{02} = \frac{1}{2}\frac{\partial^2 F_1}{\partial y^2}(x^*, y^*) = \frac{k^2 rx^*}{(1 + ky^*)^3}$$
$$a_{21} = \frac{1}{2}\frac{\partial^3 F_1}{\partial x^2 \partial y}(x^*, y^*) = \frac{ghx^*(3 - hx^{*2})}{(1 + hx^{*2})^3}\ ,\ a_{12} = \frac{1}{2}\frac{\partial^3 F_1}{\partial x \partial y^2}(x^*, y^*) = \frac{k^2 r}{(1 + ky^*)^3}$$
$$a_{30} = \frac{1}{6}\frac{\partial^3 F_1}{\partial x^3}(x^*, y^*) = \frac{ghy^*(1 - 6hx^{*2} + h^2x^{*4})}{(1 + hx^{*2})^4}\ ,\ a_{03} = \frac{1}{6}\frac{\partial^3 F_1}{\partial y^3}(x^*, y^*) = -\frac{rk^3x^*}{(1 + ky^*)^4}$$
$$b_{11} = \frac{\partial^2 F_2}{\partial y \partial x}(x^*, y^*) = \frac{mg(1 - hx^{*2})}{(1 + hx^{*2})^2}\ ,\ b_{20} = \frac{1}{2}\frac{\partial^2 F_2}{\partial x^2}(x^*, y^*) = -\frac{hmgx^*y^*(3 - hx^{*2})}{(1 + hx^{*2})^3}$$
$$b_{02} = \frac{1}{2}\frac{\partial^2 F_2}{\partial y^2}(x^*, y^*) = \frac{(p - q)}{(1 + y^*)^3}\ ,\ b_{21} = \frac{1}{2}\frac{\partial^3 F_2}{\partial x^2 \partial y}(x^*, y^*) = -\frac{hmgx^*(3 - hx^{*2})}{(1 + hx^{*2})^3}$$
$$b_{12} = \frac{1}{2}\frac{\partial^3 F_2}{\partial x \partial y^2}(x^*, y^*) = 0\ ,\ b_{30} = \frac{1}{6}\frac{\partial^3 F_2}{\partial x^3}(x^*, y^*) = -\frac{mghy^*(1 - 6hx^{*2} + h^2x^{*4})}{(1 + hx^{*2})^4}$$

Substituting the values of above expressions in first Lyapunov number and after some algebraic computations, we obtain,

$$L = -\frac{3\pi}{2bD^{\frac{3}{2}}}\frac{x^*(L_1+L_2+L_3+L_4+L_5+L_6+L_7+L_8)}{y^*\left(y^*+1\right)^2\left(hx^{*2}+1\right)^9\left(ky^*+1\right)^5}$$

where,

$$L_1 = -ghmx^{*2}y^{*2}\left(y^*+1\right)^2\left(3-hx^{*2}\right)\left(hx^{*2}+1\right)\left(ky^*+1\right)\left[g\left(ky^*+1\right)^2+kr\left(hx^{*2}+1\right)\right]^2$$
$$\left(2\alpha+h^2x^{*4}(6\alpha+gm)+2gh^2x^{*3}y^*-6ghx^*y^*-gm+2\alpha h^3x^{*6}+6\alpha hx^{*2}\right)$$

$$L_2 = 2gmx^{*2}\left(1-hx^{*2}\right)\left(hx^{*2}+1\right)\left(ky^*+1\right)^3\left(\alpha\left(hx^{*2}+1\right)^2-2ghx^*y^*\right)$$
$$\left[k^2ry^{*2}\left(y^*+1\right)^2\left(hx^{*2}+1\right)\left(\alpha+gh^2x^{*3}y^*-3ghx^*y^*+\alpha h^3x^{*6}+3\alpha h^2x^{*4}+3\alpha hx^{*2}\right)+\right.$$
$$\left.\left(ky^*+1\right)^2\left(\alpha\left(hx^{*2}+1\right)^2-2ghx^*y^*\right)^2\right]$$

$$L_3 = 2x^*y^*\left(y^*+1\right)\left(ky^*+1\right)^3\left(\alpha\left(hx^{*2}+1\right)^2-2ghx^*y^*\right)\left(g\left(ky^*+1\right)^2+kr\left(hx^{*2}+1\right)\right)$$
$$\left[\left(y^*+1\right)\left(\alpha+gh^2x^{*3}y^*-3ghx^*y^*+\alpha h^3x^{*6}+3\alpha h^2x^{*4}+3\alpha hx^{*2}\right)^2+\right.$$
$$\left.ghmx^{*2}\left(hx^{*2}+1\right)\left(3-hx^{*2}\right)\left(\alpha\left(hx^{*2}+1\right)^2-2ghx^*y^*\right)\right]$$

$$L_4 = g^2k^2m^2rx^*y^{*2}\left(y^*+1\right)\left(hx^{*2}-1\right)^2\left(hx^{*2}+1\right)^3\left(ky^*+1\right)$$
$$\left(2x^*\left(ky^*+1\right)^2\left(\alpha\left(hx^{*2}+1\right)^2-2ghx^*y^*\right)-y^*\left(y^*+1\right)\left(\left(ky^*+1\right)^2g\left(1-hx^{*2}\right)+kr\left(hx^{*2}+1\right)^2\right)\right)$$

$$L_5 = x^*\left(y^*+1\right)\left(hx^{*2}+1\right)\left(ky^*+1\right)\left(\alpha\left(hx^{*2}+1\right)^2-2ghx^*y^*\right)\left(g\left(ky^*+1\right)^2+kr\left(hx^{*2}+1\right)\right)$$
$$\left(gmy^*\left(y^*+1\right)\left(hx^{*2}-1\right)\left(ky^*+1\right)^2\left(\alpha+gh^2x^{*3}y^*-3ghx^*y^*+\alpha h^3x^{*6}+3\alpha h^2x^{*4}+3\alpha hx^{*2}\right)\right.$$
$$-x^*\left(hx^{*2}+1\right)\left(\alpha\left(hx^{*2}+1\right)^2-2ghx^*y^*\right)\left(\left(ky^*+1\right)^2g\left(1-hx^{*2}\right)+kr\left(hx^{*2}+1\right)^2\right)$$
$$\left.g^2m^2y^*\left(y^*+1\right)\left(hx^{*2}-1\right)^2\left(hx^{*2}+1\right)\left(ky^*+1\right)^2\right)$$

$$L_6 = \left(gmy^*\left(hx^{*2}+1\right)\left(1-hx^{*2}\right)\left(g\left(ky^*+1\right)^2+kr\left(hx^{*2}+1\right)\right)+2x^*\left(ky^*+1\right)^2\right.$$
$$\left.\left(\alpha\left(hx^{*2}+1\right)^2-2ghx^*y^*\right)^2\right)\left(y^*+1\right)\left(ky^*+1\right)\left(gmx^*\left(1-hx^{*2}\right)\left(hx^{*2}+1\right)\left(ky^*+1\right)^2\right.$$
$$\left(\alpha\left(hx^{*2}+1\right)^2-2ghx^*y^*\right)-\left(\alpha+gh^2x^{*3}y^*-3ghx^*y^*+\alpha h^3x^{*6}+3\alpha h^2x^{*4}+3\alpha hx^{*2}\right)$$
$$\left.\left(ky^*+1\right)^2g\left(1-hx^{*2}\right)+kr\left(hx^{*2}+1\right)^2y^*\left(y^*+1\right)\right)$$

$$L_7 = gmy^*\left(y^*+1\right)\left(1-hx^{*2}\right)\left(hx^{*2}+1\right)\left(ky^*+1\right)\left(\alpha\left(hx^{*2}+1\right)^2-2ghx^*y^*\right)$$
$$\left(-x^*\left(ky^*+1\right)^2\left(\alpha\left(hx^{*2}+1\right)^2-2ghx^*y^*\right)\left(\left(ky^*+1\right)^2g\left(1-hx^{*2}\right)+kr\left(hx^{*2}+1\right)^2\right)+\right.$$
$$gk^2mrx^{*2}y^*\left(y^*+1\right)\left(1-hx^{*2}\right)\left(hx^{*2}+1\right)^2\left(ky^*+1\right)^2+$$
$$\left.y^*\left(y^*+1\right)\left(\left(ky^*+1\right)^2g\left(1-hx^{*2}\right)+kr\left(hx^{*2}+1\right)^2\right)^2\right)$$

$$L_8 = gy^*\left(-gmy^*\left(1-hx^{*2}\right)\left(hx^{*2}+1\right)\left(g\left(ky^*+1\right)^2+kr\left(hx^{*2}+1\right)\right)+x^*\left(ky^*+1\right)^2\right.$$
$$\left.\left(\alpha\left(hx^{*2}+1\right)^2-2ghx^*y^*\right)^2\right)\left[k^2mry^*\left(y^*+1\right)^2\left(1-hx^{*2}\right)\left(hx^{*2}+1\right)^3-\right.$$

$$2hx^{*2}\left(y^*+1\right)^2\left(3-hx^{*2}\right)\left(ky^*+1\right)^3\left(\alpha\left(hx^{*2}+1\right)^2-2ghx^*y^*\right)-$$
$$hmx^{*2}\left(y^*+1\right)^2\left(3-hx^{*2}\right)\left(hx^{*2}+1\right)\left(ky^*+1\right)\left(g\left(ky^*+1\right)^2+kr\left(hx^{*2}+1\right)\right)-$$
$$3x^*\left(ky^*+1\right)\Big(-hy^*\left(y^*+1\right)^2\left(h^2x^{*4}-6hx^{*2}+1\right)\left(g\left(ky^*+1\right)^2+kr\left(hx^{*2}+1\right)\right)+$$
$$m\left(1-hx^{*2}\right)\left(hx^{*2}+1\right)\left(ky^*+1\right)^2\left(\alpha\left(hx^{*2}+1\right)^2-2ghx^*y^*\right)\Big)\Big]$$

It is difficult to show that $L = 0$ but we can assure the existence of generalized Hopf bifurcation numerically for certain choice of parameters. □

Remark: Also the system (2) undergoes Generalized Hopf bifurcation around an interior equilibrium point $E_I(x^*, y^*)$ for the pair of parameters $\{q, p\}$ and $\{q, r\}$.

7. Numerical Simulation

Numerical simulations are presented to illustrate bifurcations and examine the effects of parameter variations on the dynamics of system (2).

7.1. Codimension one bifurcation diagram

A systematic investigation of many bifurcation diagrams is conducted by varying a parameter. This allows us to get a comprehensive knowledge of how the dynamics of the system change in relation to the chosen parameter. Let us vary the parameter p, representing the mortality rate of the predator species, while keeping the other parameters fixed at $\{r = 1.65, k = 0.5, \beta = 0.13, \alpha = 0.25, g = 1.02, h = 0.44, m = 0.98, q = 1.15\}$. In Figure 4, Figure 5, Figure 6 and Figure 7 the blue solid and dotted curves represent the stable and unstable behavior of E_a, respectively. The red solid and dotted curves correspond to the stable and unstable behavior of E_I, while the green dotted curve indicates the unstable behavior of E_0. By analyzing Figure 4, it is noticed that one unstable and one stable E_I move towards each other and meet at $p = p^{(SN_2)} = 0.3212278$. Moreover, we see a similar scenario in which one unstable and one stable E_I come together and intersect at $p = p^{(SN_1)} = 0.016862$. So, the system displays two saddle-node bifurcations at the points $p = p^{(SN_1)}$ and $p = p^{(SN_2)}$. On the other hand, we see that the system's stability shifts when an interior equilibrium point meets with a predator-free equilibrium point E_a at $p = p^{(TC)} = 0.352012$. At $p = p^{(TC)}$, a transcritical bifurcation occurs, where the unstable predator-free equilibrium point becomes stable while the stable interior equilibrium point disappears. Higher mortality rate p leads to the extinction of predator species, especially when $p > p^{(TC)}$. From Figure 4, we observe that when $p < p^{(SN_1)}$ or $p^{(SN_2)} < p < p^{(TC)}$, system (2) contains one stable E_I along with unstable E_0 and E_a. Two stable and one unstable E_I, unstable E_0 and E_a are present for the system (2) when $p^{(SN_1)} < p < p^{(SN_2)}$. Due to the existence of two stable E_I in $p^{(SN_1)} < p < p^{(SN_2)}$, a bi-stability phenomenon emerges. The system has stable E_a and E_0 for $p > p^{(TC)}$.

We will now discuss how the mortality rate of predator species influences the prey and predator biomass. When $p < p^{(SN_1)}$ i.e., the mortality rate of predator species is low, then the population size of predator species is high. As a result, consumption of prey by predator species is also increase. So, population size of prey species is low. Now we slowly increase p and entering in the range $p^{(SN_1)} < p < p^{(SN_2)}$. Due to the existence of bi-stability phenomenon in $p^{(SN_1)} < p < p^{(SN_2)}$, the initial population biomass of both species determines their future population size. when $p^{(SN_2)} < p < p^{(TC)}$ i.e., an increased mortality rate leads to a reduction in predator biomass. As a result, the predation of prey decreases and prey biomass increases. When p is extremely high, i.e., $p > p^{(TC)}$, the predator species faces extinction.

Next, we consider maximal mortality rate of predator species q as bifurcation parameter. Initially, We adjust the value of parameters at $\{r = 1.65, k = 0.5, \beta = 0.13, \alpha = 0.25, g = 1.02, h = 0.44, m = 0.98, p = 0.1\}$ and vary the maximal mortality coefficient of predator q. In this bifurcation scenario, E_0 and E_a remain unstable for all q. Consequently, all bifurcations are observed by E_I. In Figure 5, we observed that one stable and one unstable E_I converge and meet at $q = q^{(SN_1)} = 1.0512027$. Also, we see a similar situation, where one unstable and one stable E_I move towards each other and meet $q = q^{(SN_2)} = 1.3547206$. As a result,

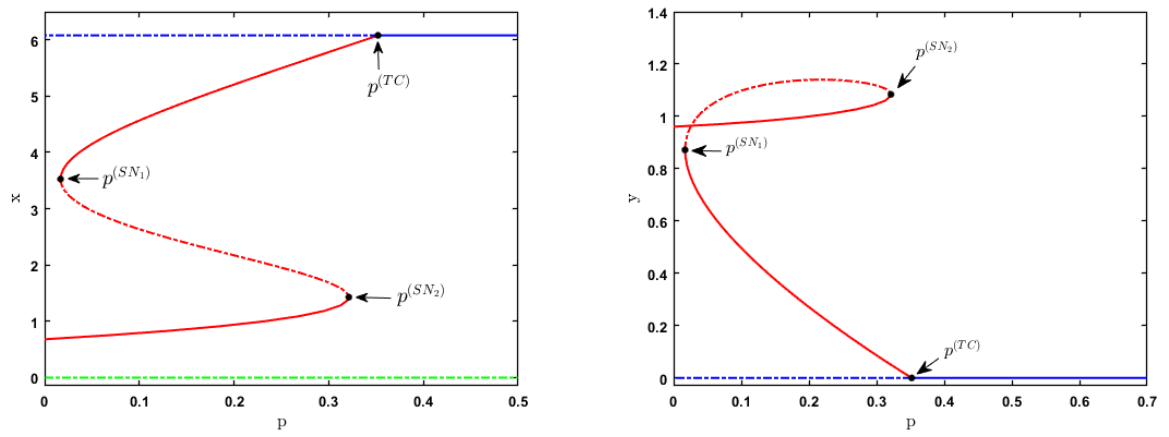

(a) p vs x (b) p vs y

Figure 4: Bifurcation diagram of system (2) with respect to p.

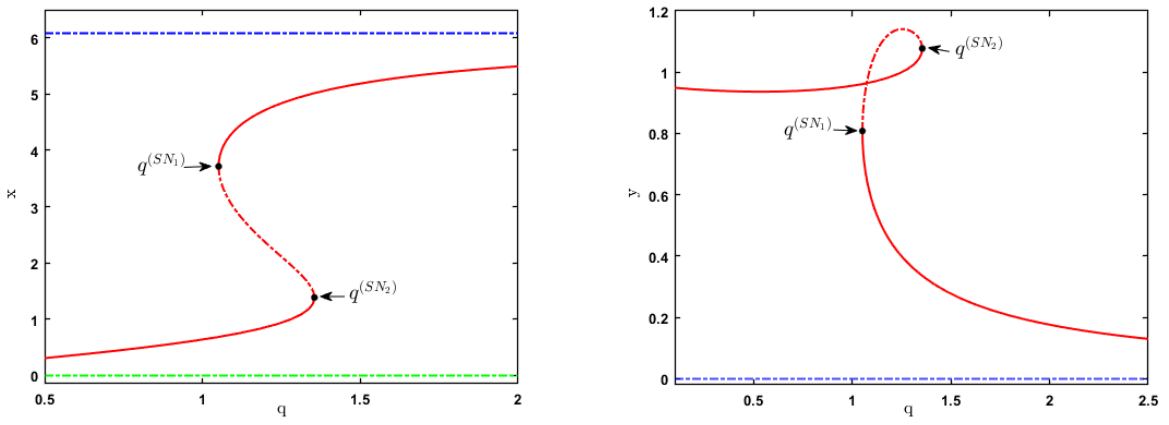

(a) q vs x (b) q vs y

Figure 5: Bifurcation diagram of system (2) with respect to q.

system (2) exhibits two saddle-node bifurcations at the points $q = q^{(SN_1)}$ and $q = q^{(SN_2)}$. It is observed that when $q < q^{(SN_1)}$ and $q > q^{(SN_2)}$, system (2) contains one stable E_I. The system has one unstable and two stable E_I for $q^{(SN_1)} < q < q^{(SN_2)}$. Due to the existence of two stable E_I in $q^{(SN_1)} < q < q^{(SN_2)}$, a bi-stability phenomenon emerges. We shall now examine how the limiting mortality rate of predator species affects the biomass of prey and predators. When the limiting mortality rate of predator species is low i.e $q < q^{(SN_1)}$,the population biomass of predator species is large. As a result, the increase in prey consumption by predator species leads to a decrease in the prey population. We gradually increase the value of q and falls into the range $q^{(SN_1)} < q < q^{(SN_2)}$. Both the population biomass is influenced by their initial biomass levels due to the bi-stability phenomena occurring in the range of $q^{(SN_1)} < q < q^{(SN_2)}$. When $q > q^{(SN_2)}$ i.e., an rise in the limiting mortality rate results in a decrease in predator biomass. Consequently, predation of prey reduces, causing an increase in prey biomass. This has ecological significance.

Now, consider another bifurcation parameter k, representing the level of fear due to predator. Initially, we set the parameter values to $\{r = 1.65, \beta = 0.13, \alpha = 0.25, g = 1.02, h = 0.44, m = 0.98, p = 0.1, q = 1.15\}$ and vary the parameter k. For any value of k, all axial equilibrium points (the trivial equilibrium point and the

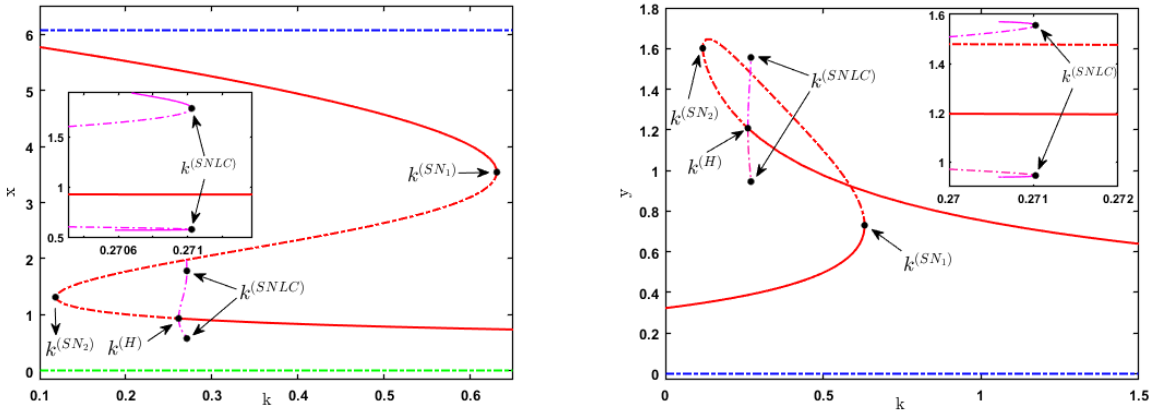

(a) k vs x (b) k vs y

Figure 6: Bifurcation diagram of system (2) with respect to k. Magenta dotted and solid curve represents the unstable and stable behaviour of limit cycle respectively.

predator-free equilibrium point) remain unstable in this bifurcation scenario. As a result, the bifurcation occurs through E_I. In Figure 6, we observe one stable and one unstable E_I move towards each other and meet at $k = k^{(SN_1)} = 0.63104307$. Additionally, a similar situation is observed between two unstable E_I at $k = k^{(SN_2)} = 0.11842867$. Consequently, the system demonstrates two saddle-node bifurcations at $k = k^{(SN_1)}$ and $k = k^{(SN_2)}$. On the other hand, one unstable E_I gain its stability at $k = k^{(H)} = 0.93320982$, resulting in a appearence of Hopf bifurcation. The hopf bifurcation is of subcritical type as the first Lyapunov coefficient is positive, which leads to the emergence of unstable bifurcating limit cycles. This cycle approach and collide with stable limit cycles at $k = k^{(SNLC)} = 0.271023$, results in the occurrence of saddle node bifurcation of limit cycles. From Figure 6, we observe that when $k < k^{(SN_2)}$ and $k > k^{(SN_1)}$, the system has one stable E_I and for $k^{(SN_2)} < k < k^{(H)}$, system (2) has two unstable and one stable E_I. One of those two unstable E_I becomes stable for $k^{(H)} < k < k^{(SN_1)}$. As a result, a bi-stability phenomenon emerges.

Next, we consider another bifurcation parameter r, representing birth rate of prey in the absence of predator. Now we vary the parameter r, while keeping the other parameters fixed at $\{k = 0.5, \beta = 0.13, \alpha = 0.25, g = 1.02, h = 0.44, m = 0.98, p = 0.1, q = 1.15\}$. In this bifurcation scenario, E_0 remain unstable for all r. As a result, the system shows bifurcation through interior equilibrium point and E_a. In Figure 7, we observed that the system change its stability when E_a meets with interior equilibrium point at $r = r^{(TC_1)} = 5.7844243$. At this point, E_a becomes unstable and a stable E_I appear. Consequently, a transcritical bifurcation occurs. This stable E_I converge and collide with another unstable E_I at $r = r^{(SN_1)} = 1.5398266$. Additionally, a similar situation is observed, where two unstable E_I move towards each other and meet at $r = r^{(SN_2)} = 2.5025307$. Consequently, system (2) experiences saddle node bifurcation at $r = r^{(SN_1)}$ and $r = r^{(SN_2)}$. On the other hand, an unstable interior equilibrium point becomes stable at $r = r^{(H)} = 2.0112076$, resulting in the occurrence of Hopf bifurcation. The hopf bifurcation is of subcritical type as the first Lyapunov coefficient is positive, which leads to the emergence of unstable bifurcating limit cycles. This cycle converges and collides with stable limit cycles at $r = r^{(SNLC)} = 1.99965$, resulting in the occurrence of a saddle node bifurcation of limit cycles. Now the stable interior equilibrium point meets with an unstable predator free equilibrium point at $r = r^{(TC_2)} = 0.15512112$. As a result, E_a becomes stable and the stable E_I vanishes at $r = r^{(TC_2)}$, a transcritical bifurcation occurs. This stable predator free equilibrium point E_a meets with E_0 at $r = r^{(BP)}$, known as branch point. From Figure 7, we observed that for $r^{(BP)} < r < r^{(TC_2)}$, system has one stable E_a and one unstable E_0. For $r^{(TC_2)} < r < r^{(SN_1)}$, the system possesses one stable E_I along with unstable E_a and E_0. When $r^{(SN_1)} < r < r^{(H)}$, two more interior equilibrium points emerge, one being stable and the other unstable. As a result, a bi-stability phenomenon arises between two stable E_I. Between those E_I, one becomes unstable for $r^{(H)} < r < r^{(SN_2)}$. When $r^{(SN_2)} < r < r^{(TC_1)}$, system has one stable E_I along

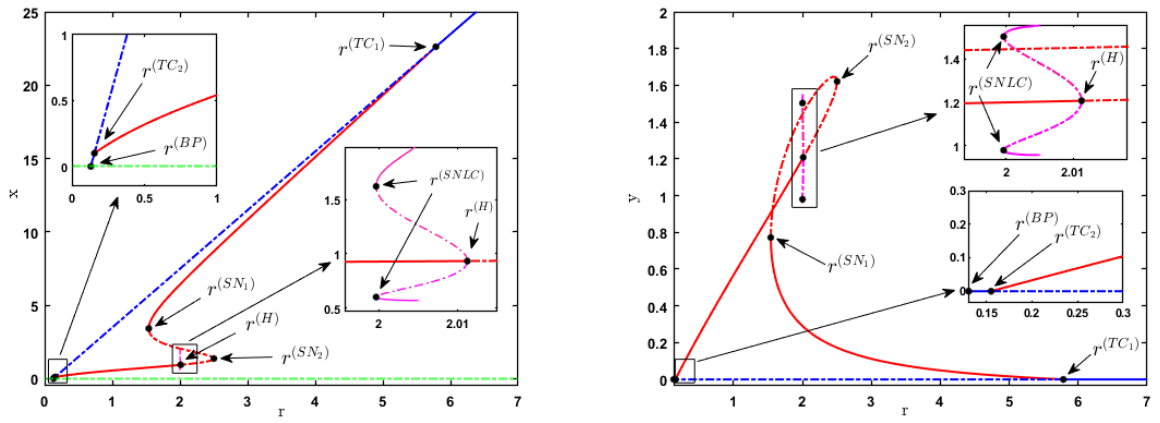

(a) r vs x (b) r vs y

Figure 7: Bifurcation diagram of system (2) with respect to r. Magenta dotted and solid curve represent the unstable and stable behaviour of limit cycle respectively.

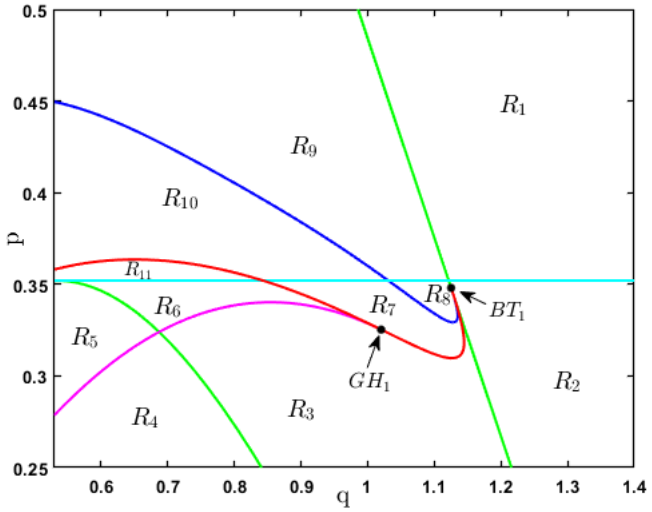

Figure 8: Two parametric bifurcation diagram of system (2) in $q - p$ parametric plane.The red curve, green curve, cyan curve, blue curve and magenta curve represents the Hopf bifurcation curve, saddle node bifurcation curve, transcritical bifurcation curve, homoclinic bifurcation curve and saddle–node bifurcation of the limit cycle curve respectively.

with unstable E_a and E_0. The stable interior equilibrium point disappear and E_a change its stability when $r > r^{(TC_2)}$.

7.2. Codimension two bifurcation diagram and Hysteresis

Previous investigations have shown that the parameter q affects the fluctuation in predator biomass and the mortality rate of predator is an important factor influencing the dynamics of the system.

Thus, for our initial analysis, we choose p and q as the bifurcation parameters and set the values of the remaining parameters to $\{r = 1.65, k = 0.5, \beta = 0.13, \alpha = 0.25, g = 1.02, h = 0.44, m = 0.98\}$. The bifurcation curves and thresholds that occur in the $q - p$ parametric plane are shown in Figure 8. These curves effectively partition the entire $q - p$ parametric plane into eleven separate regions i.e. R_1, R_2, R_3,

R_4, R_5, R_6, R_7, R_8, R_9, R_{10} and R_{11}. The following discussion will provide a more detailed examination of these regions. The figure illustrates five different types of bifurcation curves: two saddle-node curves (green), one Hopf curve (red), one homoclinic bifurcation curve (blue), one transcritical curve (cyan), and one saddle-node bifurcation of the limit cycle curve (magenta). The Hopf bifurcation curve touches the saddle–node bifurcation curve tangentially at the point $BT_1(1.1252903, 0.34802131)$ and the Hopf bifurcation curve disappears. Consequently Bogdanov–Takens bifurcation occurs. The homoclinic bifurcation curve emerges from this Bogdanov-Takens bifurcation point. Furthermore, the Hopf bifurcation curve has a generalized Hopf bifurcation point at $GH_1(1.020375, 0.32524786)$, where the saddle-node bifurcation of the limit cycle curve emerges as a consequence of the supercritical Hopf bifurcation changing into a subcritical Hopf bifurcation.

Now, we study the dynamical properties of each region. For Figure 9, Figure 11, and Figure 12, the predator and prey nullclines are represented by the red and green curves (solid), respectively. The solid blue curve shows trajectories from different initial points, denoted by black stars. The black dot signifies stability, while the circle denotes instability of the equilibrium points. In R_1, system (2) has one unstable E_0 and one stable E_a. Figure 9a shows the phase portrait and trajectories under several initial conditions for $(q, p) = (1.3, 0.45)$. Moving from R_1 to R_2, E_a becomes unstable and a stable interior equilibrium point appears through transcritical bifurcation curve. So, the system has one stable E_I along with unstable E_a and E_0 in region R_2. The phase portrait corresponding to the specific values of $(q, p) = (1.3, 0.3)$ from R_2 is shown in Figure 9b. On the other hand, when we transit from R_1 to R_9, two unstable E_I appear through saddle node curve. In R_9, one unstable E_0, one stable E_a and two unstable E_I are present. The phase portrait for R_9 is shown in Figure 9g, with an appropriate parametric value of $(q, p) = (0.9, 0.388)$. Moving from R_9 to R_8, E_a becomes unstable and a stable interior equilibrium point emerges through transcritical bifurcation curve. As a result, one stable and two unstable E_I along with unstable E_a and E_0 are present in R_8. Figure 9f represents the phase portrait for a specific value of $(q, p) = (1.1, 0.34)$. Transitioning from region R_2 to R_3, one stable and one unstable E_I emerges via saddle node curve. So, in R_3, system contain two stable and one unstable E_I, one unstable E_a and one unstable E_0. Therefore, we notice a bi-stable phenomena between between two E_I, where the population biomass of both species is influenced by their initial biomass levels. Figure 9c demonstrates the dynamical properties of R_3 with an appropriate parametric value of $(q, p) = (0.8, 0.335)$. The basin of attraction for the region R_3 is shown in Figure 10a. Moving from R_3 to R_4, one stable and one unstable E_I disappear through saddle node curve. As a result, one stable E_I, one unstable E_a and one unstable E_0 are present in R_4. The dynamic behaviour of region R_4 shown in Figure 9d for a fixed value of $(q, p) = (0.6, 0.297)$. On the other hand, when we enter from R_3 to R_7, one stable E_I undergoes a loss of stability through Hopf curve. So, the system contains one unstable E_a, one unstable E_0, two unstable and one stable E_I. The dynamical properties of R_7 with a fixed value of $(q, p) = (1.1, 0.33)$ is shown in Figure 9e. One of most intriguing phenomena occurs while shifting from region R_3 to R_6, i.e, cross saddle node bifurcation of limit cycle curve. In region R_6, A large amplitude stable limit cycle surrounds a small amplitude unstable limit cycle that surrounds an interior equilibrium point. This type of unstable limit cycle usually occurs by the existence of a subcritical Hopf bifurcation. Thus, trajectories originating within the unstable limit cycle converge towards a stable interior equilibrium point, whereas trajectories beginning from outside this unstable limit cycle converge towards high amplitude stable limit cycle. Due to presence of another stable E_I, a bi-stability phenomenon emerges in R_6 (refer to Figure 9j). Thus, the population biomass of both species is influenced by their initial biomass levels. This region exhibits both stable and unstable limit cycles, demonstrating how sensitive the system is to its initial conditions. In the long run, very different things can happen depending on small changes in the starting populations and how the species interact with each other. The basin of attraction for the region R_6 is shown in Figure 10b. A similar type of scenario observed, when we transit from R_6 to R_{11}, but their are some changes in system's dynamics. In region R_{11}, E_a becomes stable and a stable E_I disappear through transcritical bifurcation curve. As a result, a bi-stable phenomenon occurs between an interior equilibrium point and predator free equilibrium point. Therefore, based on the initial population size of both species, the trajectories either converge towards an interior equilibrium point or the predator-free equilibrium point. Figure 9k represents this dynamical properties of R_{11} for $(q, p) = (0.75, 0.355)$. Moving from R_{11} to R_{10}, a stable E_I undergoes a loss of stability through Hopf curve. This unstable interior equilibrium point surrounded by a stable limit cycle. So, the system's

dynamics lead to sustained oscillations around this unstable interior equilibrium point, demonstrating a cyclical pattern in the populations of predators and prey species. Additionally, system (2) exhibits one unstable E_I along with one stable E_a and one unstable E_0. As a result, all trajectories originating from outside the stable limit cycle either move towards a stable predator free equilibrium point or that stable limit cycle. The phase portrait corresponding to the particular values of $(q, p) = (0.75, 0.365)$ from the region R_{10} is shown in Figure 9h. Transitioning from R_4 to R_5, the system surpasses the saddle node bifurcation of limit cycle curve. As a result, there is a unique stable interior equilibrium point that is covered by an unstable limit cycle of small amplitude. This unstable limit cycle is then encompassed by a stable limit cycle of higher amplitude. The presence of such an unstable limit cycle is mainly caused by a subcritical Hopf bifurcation. Moreover, the system contains one unstable E_a and E_0. The dynamical characteristic of R_5 for a fixed value of $(q, p) = (0.6, 0.305)$ is shown in Figure 9i. We also observe that, Predator species are facing extinction in regions R_1,R_9 and R_{10} because of to their increased mortality rates. To facilitate all the characteristics of equilibrium points of each regions in $q - p$ parametric plane, see Table 2.

Table 2: Stability characteristic of equilibrium points from different regions of q vs p bifurcation, shown in Figure 8.

Regions	**Equilibrium states**	**Nature of equilibrium states**
R_1	E_0, E_a	E_0 is unstable, E_a is LAS
R_2	E_0, E_a, One interior	E_0 is unstable, E_a is unstable and other interior is LAS
R_3	E_0, E_a, Three interiors	E_0 is unstable, E_a is unstable, One interior is LAS, One interior is stable spiral and other interior is unstable
R_4	E_0, E_a, One interior	E_0 is unstable, E_a is unstable and other interior is stable spiral
R_5	E_0, E_a, One interior	E_0 is unstable, E_a is unstable and other interior is stable spiral
R_6	E_0, E_a, Three interiors	E_0 is unstable, E_a is unstable, One interior is LAS, One interior is stable spiral and other is unstable
R_7	E_0, E_a, Three interiors	E_0 is unstable, E_a is unstable, One interior is LAS, One interior is unstable spiral and other interior is unstable
R_8	E_0, E_a, Three interiors	E_0 is unstable, E_a is unstable, One interior is LAS, One interior is unstable spiral and other interior is unstable
R_9	E_0, E_a, Two interiors	E_0 is unstable, E_a is LAS, One interior is unstable spiral and other interior is unstable
R_{10}	E_0, E_a, Two interiors	E_0 is unstable, E_a is LAS, One interior is unstable spiral and other interior is unstable
R_{11}	E_0, E_a, Two interiors	E_0 is unstable, E_a is LAS, One interior is stable spiral and other interior is unstable

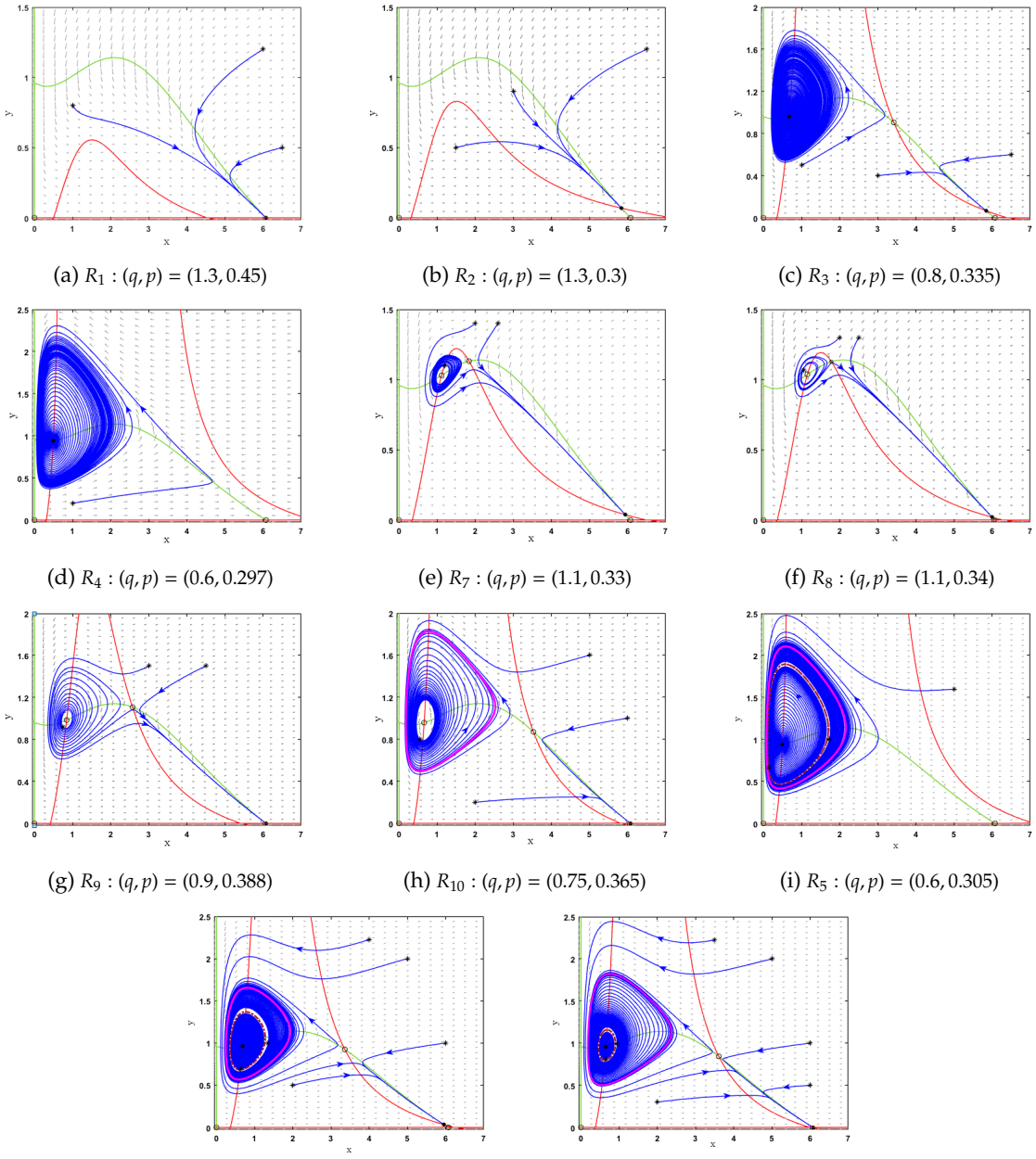

(a) $R_1 : (q, p) = (1.3, 0.45)$ (b) $R_2 : (q, p) = (1.3, 0.3)$ (c) $R_3 : (q, p) = (0.8, 0.335)$

(d) $R_4 : (q, p) = (0.6, 0.297)$ (e) $R_7 : (q, p) = (1.1, 0.33)$ (f) $R_8 : (q, p) = (1.1, 0.34)$

(g) $R_9 : (q, p) = (0.9, 0.388)$ (h) $R_{10} : (q, p) = (0.75, 0.365)$ (i) $R_5 : (q, p) = (0.6, 0.305)$

(j) $R_6 : (q, p) = (0.8, 0.343)$ (k) $R_{11} : (q, p) = (0.75, 0.355)$

Figure 9: Phase portraits for regions R_i ($i = 1, 2, 3, ...11$) of Figure 8. solid magenta curve indicates stable limit cycle and a deep red curve (dotted) indicates an unstable limit cycle.

We have noticed that system (2) exhibits homoclinic bifurcations, as seen by the blue curve in Figure 8. Figure 11 illustrates the system's dynamic evolution because of a homoclinic bifurcation, showcasing the shift of a limit cycle. Three different phase portraits are shown in this figure, representing stages before, during, and after a homoclinic bifurcation. Initially, we set the parameter value $(q, p) = (0.6, 0.305)$ in region R_{10}. Subsequently, the existence of a saddle point (interior equilibrium point) and a stable limit cycle (magenta closed orbit) around an unstable E_I indicate a pre-homoclinic bifurcation phase (Figure 11a) in

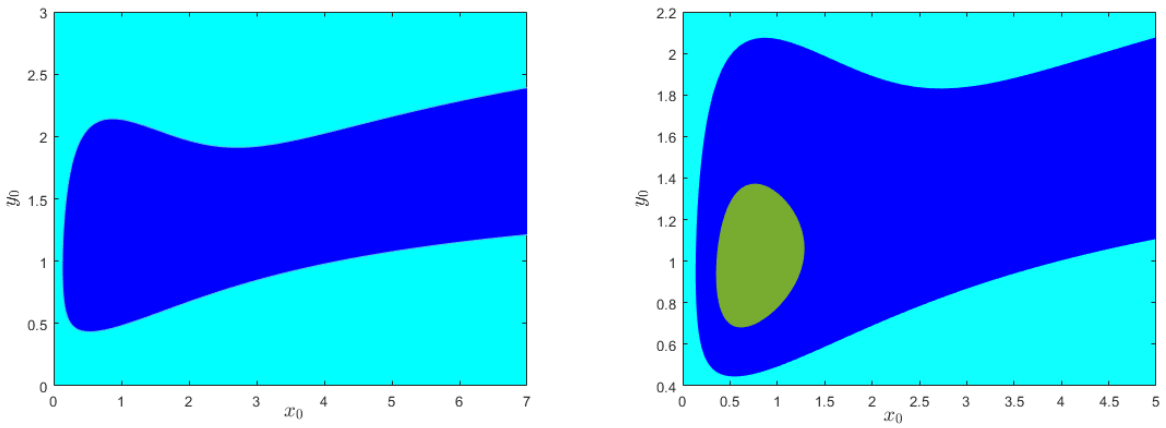

(a) Basin of attraction R_3 (b) Basin of attraction R_6

Figure 10: Basin of attraction

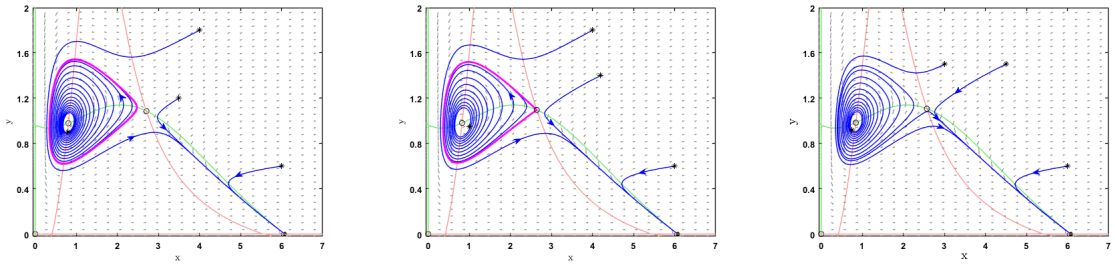

(a) $(q, p) = (0.88, 0.38)$ (b) $(q, p) \approx (0.8867291, 0.3868386)$ (c) $(q, p) = (0.9, 0.388)$

Figure 11: Phase portraits in $x - y$ plane are shown before, at, and after a homoclinic bifurcation for various values of q and p. These phase portraits illustrate the existence of a homoclinic orbit, which is represented by a magenta closed orbit in Figure 11b.

system. As bifurcation parameters (q, p) rises, the stable limit cycle expands until it perfectly meets with the saddle point. When reaching the bifurcation point at $(q, p) = (0.886729150973482, 0.386838691248586)$, the limit cycle meets the saddle point, resulting in an orbit of infinite duration (Figure 11b). This specific closed orbit is referred to as a homoclinic orbit, which establishes a connection between the saddle E_I and itself. It is important to note that it forms at the place where the stable and unstable manifolds of the saddle point intersect within the plane. If we continuously increase the value of bifurcation parameters $\{q, p\}$, the stable limit cycle and the homoclinic orbit interact, resulting in perturbations and instability in the limit cycle. Consequently, the limit cycle disappears and gives rise to the post-homoclinic bifurcation phase, as seen in Figure 11c for $(q, p) = (0.9, 0.388)$.

This bifurcation indicates a crucial situation where a slight change in the parameters q and p can move the dynamics from a stable cyclic oscillation to the extinction of predator. A similar type of scenario occurs when we move from R_7 to R_8, but there are some changes that is a slight change in the parameters q and p can move the dynamics from a stable cyclic oscillation to a stable interior equilibrium point, shown in Figure 12.

Next, we introduce maximal mortality rate of predator species, taking into account the birth rate of prey in the absence of predator. Presently, we construct two parametric bifurcation diagram in $q - r$ plane, while keeping fixed all other parameters at $\{k = 0.5, \beta = 0.13, \alpha = 0.25, g = 1.02, h = 0.44, p = 0.1, m = 0.98\}$, shown in Figure 13a.

Each type of bifurcation is represented by a different color in the illustrated figure: two saddle-node

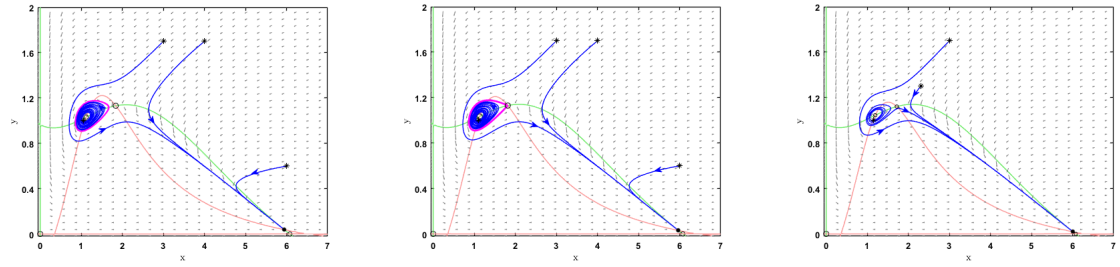

(a) $(q, p) = (1.1, 0.33)$ (b) $(q, p) \approx (1.10037794, 0.3339442)$ (c) $(q, p) = (1.11, 0.34)$

Figure 12: Phase portraits in $x - y$ plane are shown before, at, and after a homoclinic bifurcation for various values of q and p. These phase portraits illustrate the existence of a homoclinic orbit, which is represented by a magenta closed orbit in Figure 12b.

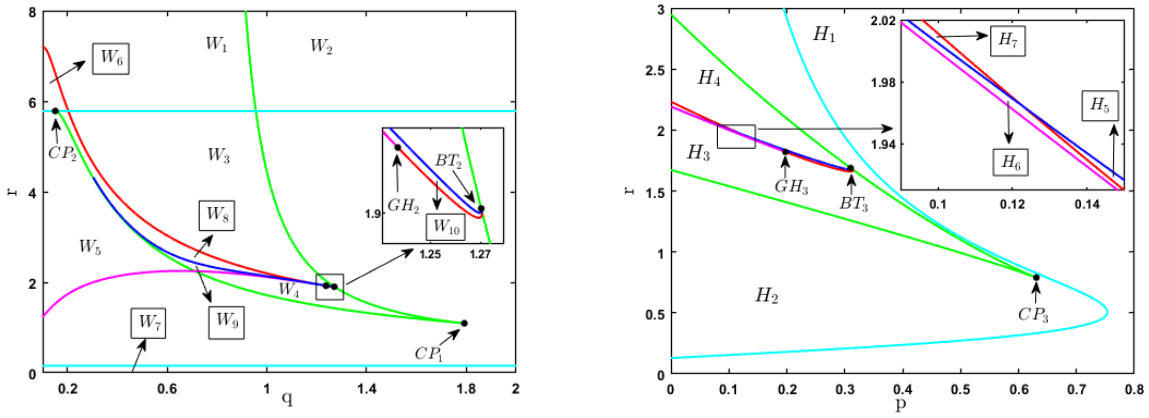

(a) q vs r (b) p vs r

Figure 13: Two parametric bifurcation diagram of system (2) in (a): $q - r$ and (b): $p - r$ parametric plane. The red curve, green curve, cyan curve, blue curve and magenta curve represents the Hopf bifurcation curve, saddle node bifurcation curve, transcritical bifurcation curve, homoclinic bifurcation curve and saddle–node bifurcation of the limit cycle curve respectively.

curves (green), one Hopf curve (red), one homoclinic curve (blue), one transcritical curve (cyan), and one saddle-node bifurcation of limit cycle curve (magenta). The entire parametric plane $q - r$ partitioned by these bifurcation curves into eleven regions, which are denoted as W_1, W_2, W_3, W_4, W_5, W_6, W_7, W_8, W_9, W_{10} and W_{11}. Several co-dimension 2 bifurcation points emerge by intersection of some of these bifurcation curves. An example of such an occurrence is a cusp bifurcation, which occurs at $CP_1(1.7921034, 1.092659)$, where two saddle node curves converge and collide, resulting in their subsequent disappearance. Another cusp bifurcation occurs at $CP_2(0.15080943, 5.784424)$, where the saddle node curve meets with transcritical curve and disappear the saddle node curve. Another co-dimension 2 bifurcation happens where the Hopf curve and the saddle–node curve meet at the point $BT_2(1.2703237, 1.9016769)$ and subsequently hopf curve vanishes. It is called the Bogdanov–Takens bifurcation. From this Bogdanov–Takens bifurcation point, the homoclinic bifurcation curve emerges, which is one type of global bifurcation. Moreover, a supercritical Hopf bifurcation transform into a subcritical Hopf bifurcation at $GH_2(1.2370357, 1.9229855)$, known as generalized hopf bifurcation point (lie on hopf curve). As a result, saddle-node bifurcation of limit cycles curve emerges from this bifurcation point. All the characteristics of equilibrium points of each regions in $q - r$ parametric plane are described in Table 3.

Table 3: Stability characteristic of equilibrium points from different regions of q vs r bifurcation, shown in Figure 13a.

Regions	**Equilibrium states**	**Nature of equilibrium states**
W_1	E_0, E_a, Two interiors	E_0 is unstable, E_a is LAS, One interior is unstable spiral and other interior is unstable
W_2	E_0, E_a	E_0 is unstable, E_a is LAS
W_3	E_0, E_a, Three interiors	E_0 is unstable, E_a is unstable, One interior is LAS, One interior is unstable spiral and other interior is unstable
W_4	E_0, E_a, Three interiors	E_0 is unstable, E_a is unstable, One interior is LAS, One interior is stable spiral and other is unstable
W_5	E_0, E_a, One interior	E_0 is unstable, E_a is unstable and other interior is stable spiral
W_6	E_0, E_a, Two interiors	E_0 is unstable, E_a is LAS, One interior is stable spiral and other interior is unstable
W_7	E_0, E_a	E_0 is unstable, E_a is LAS
W_8	E_0, E_a, Three interiors	E_0 is unstable, E_a is unstable, One interior is LAS, One interior is stable spiral and other is unstable
W_9	E_0, E_a, Three interiors	E_0 is unstable, E_a is unstable, One interior is LAS, One interior is stable spiral and other is unstable
W_{10}	E_0, E_a, Three interiors	E_0 is unstable, E_a is unstable, One interior is LAS, One interior is unstable spiral and other interior is unstable
W_{11}	E_0, E_a, One interior	E_0 is unstable, E_a is unstable and other interior is LAS

Additionally, we explore the dynamical properties along with bifurcation thresholds in $p - r$ parametric plane to examine the system in different point of view. Figure 13b represents the corresponding bifurcation diagram in $p - r$ plane, with all other parameters fixed at $\{k = 0.5, \beta = 0.13, \alpha = 0.25, g = 1.02, h = 0.44, q = 1.15, m = 0.98\}$. This figure shows numerous bifurcation curves, each representing a distinct type of bifurcation: two saddle-node curves in green, one Hopf curve in red, one homoclinic curve in blue, one transcritical curve in cyan, and one saddle-node of the limit cycle curve in magenta. The parametric plane $p - r$ is separated by these bifurcation curves into seven regions, denoted as H_1, H_2, H_3, H_4, H_5, H_6 and H_7. Several co-dimension 2 bifurcation points are formed when some of these bifurcation curves meet. An instance of such phenomenon is a cusp bifurcation that takes place at $CP_3(0.63077854, 0.78939536)$, where the convergence and collision of two saddle node curves result in their subsequent disappearance. On the other hand, generalized hopf bifurcation point appear on hopf curve at $GH_3(0.19752392, 1.8203157)$, where subcritical hopf bifurcation transforms into supercritical hopf bifurcation. This hopf bifurcation curve meets saddle node bifurcation curve at $BT_3(0.31015925, 1.6882354)$ and disappears, which leads to the

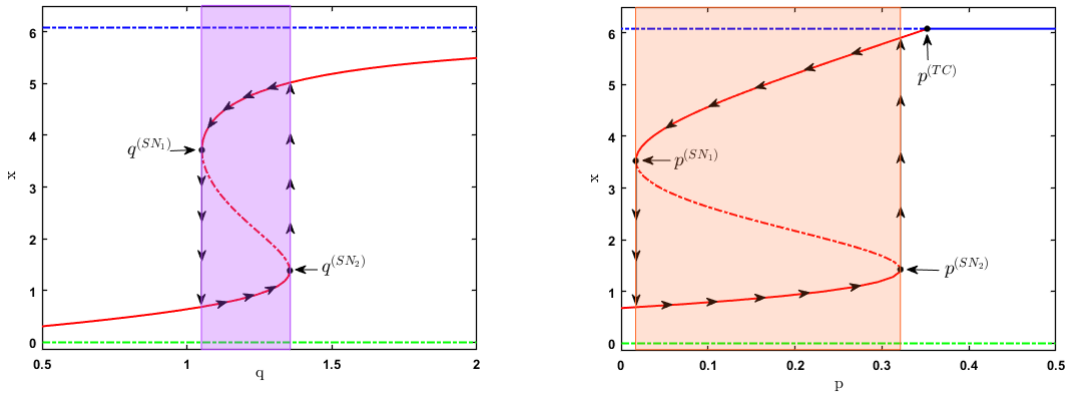

(a) hysterisis loop for q vs x

(b) hysterisis loop for p vs x

Figure 14: Evidence of hysteresis phenomenon for the parameter q and p. The red solid and dotted curves represent the stable and unstable behaviour of E_I.

occurrence of Bogdanov-Takens bifurcation. All the characteristics of equilibrium points of each regions in $p - r$ parametric plane are described in Table 4.

Table 4: Stability characteristic of equilibrium points from different regions of p vs r bifurcation, shown in Figure 13b.

Regions	**Equilibrium states**	**Nature of equilibrium states**
H_1	E_0, E_a	E_0 is unstable, E_a is LAS
H_2	E_0, E_a, One interior	E_0 is unstable, E_a is unstable and other interior is stable spiral
H_3	E_0, E_a, Three interiors	E_0 is unstable, E_a is unstable, One interior is LAS, One interior is stable spiral and other is unstable
H_4	E_0, E_a, Three interiors	E_0 is unstable, E_a is unstable, One interior is LAS, One interior is unstable spiral and other interior is unstable
H_5	E_0, E_a, Three interiors	E_0 is unstable, E_a is unstable, One interior is LAS, One interior is unstable spiral and other interior is unstable
H_6	E_0, E_a, Three interiors	E_0 is unstable, E_a is unstable, One interior is LAS, One interior is stable spiral and other is unstable
H_7	E_0, E_a, Three interiors	E_0 is unstable, E_a is unstable, One interior is LAS, One interior is stable spiral and other is unstable

Hysteresis refers to the phenomenon where the behavior of prey biomass does not simply follow the changes in predator mortality rates (q and p) in a straightforward manner. Instead, the system exhibits a history-dependent response. As the mortality rate of the predator species q increases, the prey biomass moves along a specific equilibrium path. However, when the mortality rate is decreased again, the prey biomass does not retrace its previous path. Instead, it follows a different trajectory, forming a loop-like behavior, shown in Figure 14a.

This occurs because, as q reaches certain critical values (at saddle-node bifurcations $q^{(SN_1)}$ and $q^{(SN_2)}$), the stable and unstable equilibrium points in the system collide and vanish. Once this happens, the system cannot simply return to its original state, even if q is reversed to its initial value. Instead, the system shifts toward the nearest available equilibrium, creating a path-dependent cycle.

A similar dynamic is observed when the mortality rate of the predator species p fluctuates. The prey biomass does not immediately return to its original state after the mortality rate of p is restored. Instead, the system exhibits a lagged response, following a different equilibrium path, which also leads to a looping

behavior, shown in Figure 14b.

8. Conclusion

Ecological study focuses on understanding the ecosystem's dynamic complexity and identifying the ecological components that influence it. In recent years, several mathematical models have been developed to investigate the various ecological dynamics [20] under different environmental conditions. One example of an ecological model is the prey-predator interaction model. An extensive experiment of a prey-predator model, including different biological or physiological parameters, helps to discover the key elements that play a significant role in determining the community structure and preserving biodiversity. Fear [21, 2, 22, 23, 24] is a physiological element experienced by prey in response to predators. Many experiments have shown that the presence of predators can change the behavior of prey species, leading to a more effective reduction in prey biomass than direct predation [25]. On the other hand, the mortality rate of predator species plays a vital role in the growth of the prey population. Here, we have considered the mortality rate of predators in the absence of prey, which is a bounded function but also is an increasing function of predator biomass. The present study introduces a prey-predator model that incorporates the impact of fear produced by predator species on prey species and the specific mortality rate of predator species. The suggested model includes the Holling type-IV functional response and intraspecific competition of prey to make the dynamics more plausible.

First, we have confirmed the well-posedness of our suggested model by demonstrating that solutions remain positive and confined in a specific region $B \subseteq \mathbb{R}^2_+$. Subsequently, we have analyzed the local dynamics of the associated system. The system always shows an unstable E_0 along with a predator-free equilibrium point E_a. The stability condition of E_a have been discussed in theorem (5.2). Additionally, the system comprises of interior equilibrium points (E_I), the quantity and presence of which depend upon several types of factors explained in section (4.2). The stability condition of E_I is discussed in the theorem (5.3). The present study primarily focuses on two key factors: the level of fear k of prey species and the limiting mortality rate q of predator species. In addition, we have included the mortality rate p of predator species and the birth rate r of prey species. Then we have examined how the dynamics of system are affected by the fluctuations of parameters k, q, p and r. By conducting a numerical analysis, we have demonstrated that the system undergoes two saddle-node bifurcations for the parameters q, p, k and r, as well as one transcritical bifurcation for the parameter p. The system undergoes one subcritical hopf bifurcation and saddle-node bifurcation of limit cycles with respect to the parameters k and r. Under some specific parametric values, the system can show a bi-stable phenomenon between two E_I. In some cases, a bi-stable phenomenon can also occur between an E_I and E_a. We have observed some changes in the prey-predator population when we varied some bifurcation parameters of the system (2). For example, the predator species faces extinction at a higher mortality rate, and the prey population decreases when the level of fear by predators increases. We have also examined two parametric bifurcations and observed that the $q-p$ parametric plane exhibits both Bogdanov-Takens and Generalized Hopf bifurcation. Furthermore, the parametric plane $q-p$ exhibits homoclinic bifurcation. Moreover, we have also examined two parametric bifurcation diagrams in $q-r$ and $p-r$ planes, which are cusp bifurcation, Bogdanov-Takens bifurcation, Generalized Hopf bifurcation and Homoclinic bifurcation. Furthermore, a hysteresis cycle has been observed in prey population due to the variations in the mortality rate of predator species and maximal mortality of predator species, as stated in section 7.2. From the bifurcation analysis, we observe certain changes in the prey and predator populations, given below:

(i) When the mortality rate of predator species p is low, the predator population size is large. This leads to an increase in the consumption of prey by the predators. Gradually raising the mortality rate of the predator species reveals that the population sizes of both predator and prey become dependent on their initial population sizes. However, when the mortality rate of the predator species p is high, the predator population declines, eventually leading to extinction. As a result, the prey population reaches its maximum level.

(ii) when the maximal mortality q of predator species is low, then the size of prey population low due to high predation pressure. Gradually raising q reveals that the population sizes of both predator and prey depends on their initial population biomass. However, when q is high, the predator population decreases but does not go extinction, leading to a decrease in predation pressure and an increase in the prey population size.

A thorough analysis of this model could offer valuable insights into population dynamics in real-world scenarios. Future enhancements to the model could incorporate two prey species and one predator, which would greatly contribute to preserving biodiversity and maintaining community structure.

Novelty of this work

(i) As the predator population increases and closes to the environment's carrying capacity, maximal mortality (q) starts effecting.
(ii) By shifting the interior equilibrium point E_I to the origin and applying certain transformations, the theorems for generalized Hopf and Bogdanov-Takens bifurcation have been proved.
(iii) The system exhibits homoclinic bifurcation and saddle node bifurcation of limit cycles for the changes in both the parameters p and q, where p and q represents mortality of predator at initial density and maximal mortality of predator respectively.
(iv) A hysterisis loop is shown in prey biomass with respect to parameters p and q.

Funding

This research received no external funding.

Conflict of Interest

With reference to this study, the authors claim that they do not have any conflict of interest.

Author contributions

All the authors have participated equally in all the aspects of this paper: conceptualization, methodology, investigation, formal analysis, writing-original draft preparation, writing-review and editing.

Availability of data and materials

The data used to support the findings of the study are available within the article.

Acknowledgements

The first author (Nirmalya Mondal) is thankful to the Council of Scientific & Industrial Research, India for providing JRF, and the second author (Souvick Karmakar) is thankful to the Ministry of Social Justice and Empowerment, Government of India for providing Fellowship.

References

[1] R. P. Agarwal, O. Bazighifan, and M. A. Ragusa, 2021, *Nonlinear neutral delay differential equations of fourth-order: oscillation of solutions*, Entropy, 23(2):129.

[2] Amartya Das and GP Samanta. 2018, "Modeling the fear effect on a stochastic prey–predator sys- tem with additional food for the predator.". *Journal of Physics A: Mathematical and Theoretical*, **51(46):465-601**.

[3] A. Duro, V. Piccione, M. A. Ragusa, and V. Veneziano. 2014, "New enviromentally sensitive patch index-espi-for medalus protocol". *American Institute of Physics*, **1637**: 305–312.

[4] Guirong Jiang and Qishao Lu and Linning Qian. 2007, "Complex dynamics of a Holling type II prey–predator system with state feedback control". *Chaos, Solitons & Fractals*, **31(2)**: 448-461.

[5] Zhihua Liu and Rong Yuan. 2004, "Stability and bifurcation in a delayed predator–prey system with Beddington–DeAngelis functional response". *Journal of Mathematical Analysis and Applications*, **296(2)**: 521-537.

[6] C. S. Holling. 2004 "Some characteristics of simple types of predation and parasitism". *The canadian entomologist*, **91(7)**: 385-398.

[7] Jai Prakash Tripathi and Swati Tyagi and Syed Abbas. 2016, "Global analysis of a delayed density dependent predator–prey model with Crowley–Martin functional response". *Communications in Nonlinear Science and Numerical Simulation*, **30(1)**: 45-69.

[8] Souvick Karmakar, Parvez Akhtar, Debgopal Sahoo and Guruprasad Samanta. 2024, "Dynamical analysis of a predator-prey model in toxic environment with strong reproductive Allee effect". *Filomat*, **38(10)**: 3597-3626.

[9] M. Cavani and M. Farkas. 1994, "Bifurcations in a predator-preymodel with memory and diffusion. I: andronov-Hopf bifurcation". *Acta Mathematica Academiae Scientiarum Hungaricae*, **63(3)**: 213-229.

[10] Juan Ye and Yi Wang and Zhan Jin and Chuanjun Dai and Min Zhao. 2022, "Dynamics of a predator-prey model with strong Allee effect and nonconstant mortality rate". *Mathematical Biosciences and Engineering*, **19(4)**: 3402-3426.

[11] Xiaoying Wang, Liana Zanette, and Xingfu Zou, 2016 "Modelling the fear effect in predator–prey inter- actions". *Journal of mathematical biology* **73(5)**: 1179–1204.

[12] Liana Y Zanette, Aija F White, Marek C Allen, and Michael Clinchy, 2011"Perceived predation risk reduces the number of offspring songbirds produce per year" *Science*.**334(6061)**: 1398–1401

[13] Alessandro Arsie and Chanaka Kottegoda and Chunhua Shan. 2022, "A predator-prey system with generalized Holling type IV functional response and Allee effects in prey". *Journal of Differential Equations*, **309**: 704-740.

[14] Parvez Akhtar, Souvick Karmakar, Debgopal Sahoo and Guruprasad Samanta. 2024, "Dynamical analysis of a prey–predator model in toxic habitat with weak Allee effect and additional food". *International Journal of Dynamics and Control*.

[15] S.L.Ross, 1984 "Differential Equations". *Springer*.

[16] B. Anderson, J. Jackson, and M. Sitharam, 1998. "Descartes' rule of signs revisited.". *The American Mathematical Monthly*, **105(5)**: 447–451.

[17] L. Perko, 2013. "Differential equations and dynamical systems, volume 7" *Springer Science & Business Media*..

[18] J. D. Murray, 2003. "Mathematical Biology: II: Spatial Models and Biomedical Applica- tions, volume 3." *Springer*.

[19] Yuri A. Kuznetsov, 2007. "Elements of applied bifurcation theory, " *Springer* (second edition),**112**.

[20] V. Piccione, M. A. Ragusa, V. Rapicavoli, and V. Veneziano, 2018. " Monitoring of a natural park through espi." *AIP Conference Proceedings, volume 1978, page 140005. AIP Publishing LLC.*

[21] Scott Creel, David Christianson, Stewart Liley, and John A Winnie Jr, 2007. "Predation risk affects reproductive physiology and demography of elk.". *Science* **315(5814)**: 960–960.

[22] Meghadri Das and GP Samanta, 2020. "A delayed fractional order food chain model with fear effect and prey refuge.". *Mathematics and Computers in Simulation* **178**: 218–245.

[23] Sudeshna Mondal and GP Samanta, 2020." Dynamics of a delayed predator–prey interaction incorporating nonlinear prey refuge under the influence of fear effect and additional food". *Journal of Physics A: Mathematical and Theoretical*, **53(29)**: 295-601.

[24] Sudeshna Mondal, Alakes Maiti, and GP Samanta, 2018."Effects of fear and additional food in a delayed predator–prey model." *Biophysical Reviews and Letters*, **13(04)**: 157–177.

[25] Bijoy Kumar Das, Debgopal Sahoo and G.P. Samanta, 2022"Impact of fear in a delay-induced predator–prey system with intraspecific competition within predator species.". *Mathematics and Computers in Simulation* **191**: 134–156.